NeuroImage 243 (2021) 118503

Contents lists available at ScienceDirect

NeuroImage

journal homepage: www.elsevier.com/locate/neuroimage

Advances in resting state fMRI acquisitions for functional connectomics

Luisa Raimondo[a,b], Ícaro A.F. Oliveira[a,b], Jurjen Heij[a,b], Nikos Priovoulos[a], Prantik Kundu[c,d], Renata Ferranti Leoni[e], Wietske van der Zwaag[a,*]

[a] Spinoza Centre for Neuroimaging, Amsterdam, the Netherlands
[b] Experimental and Applied Psychology, VU University, Amsterdam, the Netherlands
[c] Hyperfine Research Inc, Guilford, CT, United States
[d] Icahn School of Medicine at Mt. Sinai, New York, United States
[e] InBrain, Department of Physics, FFCLRP, University of São Paulo, Ribeirão Preto, Brazil

ARTICLE INFO

Keywords:
Resting state
Functional connectome
Echo planar imaging
ME-EPI
High field

ABSTRACT

Resting state functional magnetic resonance imaging (rs-fMRI) is based on spontaneous fluctuations in the blood oxygen level dependent (BOLD) signal, which occur simultaneously in different brain regions, without the subject performing an explicit task. The low-frequency oscillations of the rs-fMRI signal demonstrate an intrinsic spatiotemporal organization in the brain (brain networks) that may relate to the underlying neural activity. In this review article, we briefly describe the current acquisition techniques for rs-fMRI data, from the most common approaches for resting state acquisition strategies, to more recent investigations with dedicated hardware and ultra-high fields. Specific sequences that allow very fast acquisitions, or multiple echoes, are discussed next. We then consider how acquisition methods weighted towards specific parts of the BOLD signal, like the Cerebral Blood Flow (CBF) or Volume (CBV), can provide more spatially specific network information. These approaches are being developed alongside the commonly used BOLD-weighted acquisitions. Finally, specific applications of rs-fMRI to challenging regions such as the laminae in the neocortex, and the networks within the large areas of subcortical white matter regions are discussed. We finish the review with recommendations for acquisition strategies for a range of typical applications of resting state fMRI.

1. Introduction

Resting state functional magnetic resonance imaging (rs-fMRI) studies spontaneous fluctuations in the BOLD signal, which are synchronous between spatially distinct brain regions in the absence of a specific task, to infer functional connectivity (Jann et al., 2016; Lee et al., 2013; Smith et al., 2013). Biswal et al. (1995) first showed these coherent spontaneous fluctuations in the somatosensory areas, and this work was quickly followed by other brain systems (visual, auditory, cognitive (for a review, see van den Heuvel and Hulshoff Pol, 2010)). Functional connectivity has since then been shown to provide reproducible resting state brain networks both at individual and group levels (Yang et al., 2020). The most relevant are the default mode (DMN), motor, visual, auditory, language, and attentional networks (Yeo et al., 2011). Resting State Networks can only be obtained if sufficient quality data is acquired, covering all the brain areas of interest, either with the standard BOLD contrast, or a suitable alternative. The requirement to image specific brain areas of interest, or practical limitations in scan time or scanner availability may limit the available choices for acquisition. Practical considerations must be taken into account for the robust application of rs-fMRI.

In this review, we first discuss general recommendations or common strategies for rs-fMRI in section 2 before discussing the possibilities offered by ultra-high field in section 3, and possibilities that open up with other hardware improvements such as improved rf-coils and gradients in section 4 New or promising sequences used for rs-fMRI for connectomics are discussed in sections 5 to 7, detailing fast acquisitions, multi-echo echo planar imaging (EPI) and alternative contrasts, respectively. Finally, we discuss two 'new' brain areas targeted by rs-fMRI in sections 8 and 9: cortical laminae and white matter. We finish the review with recommendations for acquisition strategies for a range of typical applications of resting state fMRI, summarized in Table 1.

2. General acquisition

Currently, 3 Tesla (3T) is the most convenient field strength for acquiring reliable data from large cohorts on clinical scanners, often using gradient-echo echo-planar imaging (GE-EPI) sequences (Smith et al., 2013). These acquisitions are fast, covering an entire brain in a few sec-

* Corresponding author.
E-mail address: w.vanderzwaag@spinozacentre.nl (W. van der Zwaag).

https://doi.org/10.1016/j.neuroimage.2021.118503.
Received 26 February 2021; Received in revised form 16 August 2021; Accepted 22 August 2021

onds, and naturally T2* weighted, and therefore highly efficient. The T2* weighting makes them sensitive to the Blood Oxygen level Dependent (BOLD) signal of interest. BOLD signal is based on oxygen concentration changes in the blood that lead to changes in T2 and T2*; however, T2* is more affected. Therefore, GE sequences are commonly used despite the more significant effects of large vessels compared to T2-weighted spin-echo sequences (Yacoub et al., 2005).

Whole-brain coverage, including the entire cerebellum, is required, with in-plane resolution as high as possible (typically about 2 to 3 mm) and a TR of 2 to 3 s (Van Dijk et al., 2010). Such parameters are feasible on commercial scanners used in standard clinical routine. However, higher temporal resolution provides a better sampling of physiological artifacts that can then be filtered out (Jahanian et al., 2019), as discussed in sections 4 and 5. Multi-band imaging techniques, which will be discussed in section 5, enable the acquisition of images with subsecond temporal resolutions (Smith et al., 2013; Yang et al., 2020), like the ones for the Human Connectome Projects (HCP) in Development and Aging (72 slices with 2-mm isotropic voxels, TR = 800 ms) (Harms et al., 2018).

Another factor to consider when designing rs-fMRI studies is the duration of the run. Acquisition times of about 6 minutes have provided adequate sampling to obtain robust functional connectivity since estimates of correlation strengths stabilize before this time (Van Dijk et al., 2010). However, longer scan times are required when low spatial smoothing is used (~ 2 mm), and small seed regions are employed (Caparelli et al., 2019). Unreliable connections between two specific regions can be better measured with multiple scans per subject (Pannunzi et al., 2017). This approach also allows a margin of error for exclusion of data due to scanner transients and head motion. Therefore, when possible, longer acquisitions (about 12 min), split into short (6 min) runs are recommended (Hacker et al., 2019). For children, who typically do not tolerate staying in the same position for long times, multiple (4 to 6), even shorter runs (about 3.5 min) can be acquired (Harms et al., 2018).

During resting state experiments, participants are usually instructed to keep their eyes closed (EC), eyes open (EO), or eyes fixated on a crosshair (EO-F). Although EO and EO-F produce similar functional connectivity results (Van Dijk et al., 2010), several studies have shown significant differences between eyes open and closed, reporting BOLD signal with decreased amplitude and lower variance in the former condition (Donahue et al., 2012; Jao et al., 2013; Xu et al., 2014). Dynamic changes in connectivity patterns are also dependent on eye conditions (Agcaoglu et al., 2020). Recently, functional connectivity within the visual networks was shown to present pronounced differences between EC and EO-F in a large dataset, while only EO-F functional connectivity showed significant correlations with age, gender, and social status score (Agcaoglu et al., 2019). Greater reliability of within-network connections was reported when participants were lying still with their eyes fixated on a cross (Patriat et al., 2013; Zou et al., 2015). Eye- movements are better controlled, and the brain seems less active with visual fixation (Weng et al., 2020). Therefore, EO-F is a more controlled condition that reduces experimental variability and appears to be a better choice for collecting rs-fMRI data and correlating functional connectivity with demographic and behavioral variables (Agcaoglu et al., 2019).

Although these are the most common methodologies for rs-fMRI, advances in hardware, field strength, pulse sequences, image processing and analysis have allowed other approaches that enable new applications, such as laminar connectivity.

3. High field MRI

As mentioned, currently most resting state fMRI data are acquired at 3T. Nevertheless, the increasing availability of 7T and even higher field scanners may provide advantages for rs-fMRI (Hale et al., 2010). Fig. 1 clearly shows that, regardless of the spatial smoothing, 7T networks show higher correlation coefficients. Obtaining reliable connectivity patterns with less smoothing means that the spatial characteristics of the networks can be measured with greater spatial specificity than at lower field. This can be further increased by exchanging signal for increased spatial resolution of the acquired data.

The main advantage of ultra-high field fMRI is the availability of higher spatial specificity through higher spatial resolution, which facilitates the interpretation of the functional maps with respect to the underlying neuronal activity. When smaller imaging units (i.e. voxels) are sampled, partial volume effects decrease (Yacoub et al., 2001), but also the SNR and functional CNR (fCNR) are reduced. Ultra-high fields are advantageous because of the linear dependency of the SNR on the magnetic field (Pohmann et al., 2016; Vaughan et al., 2001) and the supralinear gains in BOLD fCNR (van der Zwaag et al., 2009; Yacoub et al., 2001). These combined effects greatly improve signal detection, allowing higher spatial resolution, and a better spatial accuracy of the fMRI maps. However, higher spatial resolution implies longer TR, as a larger number of slices is required to cover the brain. Resting state studies need whole-brain measurements to detect functional networks completely, as these are largely distributed across the brain, including the cerebellum (Buckner et al., 2011). By combining a relatively standard 2D-EPI acquisition with parallel imaging at 7T, De Martino and colleagues (De Martino et al., 2011) showed that enough sensitivity can be retained to extract the typical resting state networks, even at high spatial resolutions of 1 mm isotropic voxels, without sacrificing whole brain coverage or temporal resolution (2 s). The smaller voxel volumes reduce partial volume effects and leads to more distinct spatial features, allowing improved localization of the resting state networks (Newton et al., 2012).

High fields present several technical and methodological challenges, such as inhomogeneous B0, receive and transmit RF coil sensitivity profiles (Van de Moortele et al., 2009; Yang et al., 2002). The advent of multi-channel receive coils and parallel imaging techniques (Setsompop et al., 2016), along with improved gradient performances and correction for field inhomogeneities (Togo et al., 2017; Van de Moortele et al., 2009) now allow large volume fMRI acquisition at high fields (see also section 4). Novel analysis approaches can improve the analysis of ultra-high fields resting state fMRI, such as using a cluster-based physiological noise correction (Pinto et al., 2017), or connective field mapping (Knapen, 2021). Physiological noise mitigation, which is especially important at higher fields (Triantafyllou et al., 2011), will be discussed in the fast imaging section as it is somewhat sequence dependent.

As the technical challenges associated with ultra-high field are being solved, fMRI becomes possible beyond 7 T also, which should further increase the SNR and CNR gains. For example, Yacoub et al. (2020) used a 10.5T scanner to acquire resting state data in macaques. They demonstrate that the combination of multi-channel transmit and receiver arrays, optimized pulse sequences, and a careful anesthesia regime allows for detailed single-subject resting state analysis at high resolutions (0.75 mm isotropic), and they detected robust resting state networks across individual macaques, which closely resembled human findings.

Despite the advantages of ultra-high field fMRI in terms of SNR, CNR and parallel imaging performance, fMRI applications are hindered by the quadratically-increasing Specific Absorption Rate (SAR). SAR limitations can restrict fMRI EPIs when using multiband pulses, refocusing pulses as in SE-EPI, high spatial- or temporal-resolution, fat saturation or parallel transmit systems (pTX). SAR efficiency can be improved by new coil designs (Ertürk et al., 2017; Lee et al., 2012; Wu et al., 2016), SAR-optimizing pTX techniques (Poser et al., 2014), advanced multiband pulses, such as PINS (Hargreaves et al., 2004; Norris et al., 2011) and lower-SAR fat saturation (Stirnberg et al., 2016). More specifically for resting state measurements, in 2012 Koopmans et al. implemented a low-SAR PINS pulse with which they could perform a whole-brain spin-echo resting-state experiment (Koopmans et al., 2012). A group-level independent component analysis (ICA) revealed several resting-state networks, highlighted by the higher specificity and sensitivity in higher susceptibility regions. Today, high SAR techniques are regularly used in

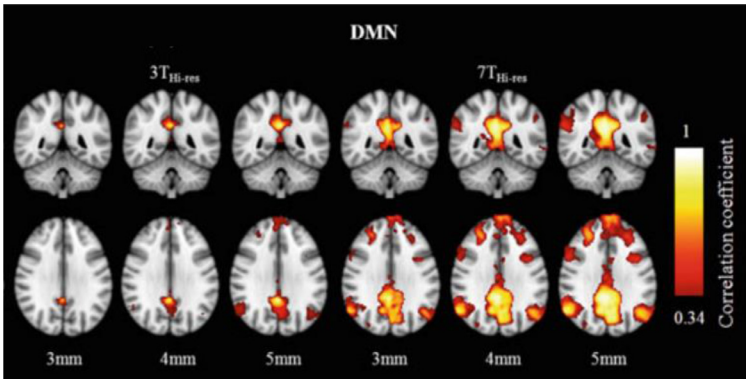

Fig. 1. Functional connectivity maps of the default mode network (DMN) of a representative subject, overlaid on the standard MNI brain. 3, 4 and 5 mm denote the FWHM of the spatial smoothing kernel applied prior to correlation computation. $3T_{high\text{-}res}$ represents data acquired with 3T and $7T_{high\text{-}res}$ with 7T, with the same spatial resolution (for comparison). Figure adapted with permission from (Hale et al., 2010).

ultra-high field fMRI (Gras et al., 2019; Huber et al., 2018; Ivanov et al., 2017; Wald, 2012).

By now, many resting state studies have been conducted using ultra-high field MRI. Some of these will be discussed in other sections because of the advanced sequences or contrast used. The higher SNR and better spatial resolution provided by ultra-high field strengths are well suited to assess the temporal reliability of mapping results, and to determine if resting-state fMRI can be applied in a clinical setting. For example, Branco et al. (2018) used resting state fMRI at 7T to examine two functional networks of major importance in preoperative planning (sensorimotor and language networks) and assessed their intrasession and intersession temporal reliability. Torrisi et al. (2017) used 7T rs-fMRI to map the habenula resting state network at high resolution in humans, to investigate its involvement in disorders such as anxiety, pathophysiology of depression and addiction disorders. Ebneabbasi et al. (2020) assessed the brain–behavior correlations between the emotion processing- and emotion regulation-related areas and the level of depression severity.

Ultra-high field resting state MRI may also offer insights in fundamental neuroscience, for example to map connectivity within the human visual cortex (Heinzle et al., 2011; Raemaekers et al., 2014), as well as in studying layer specific connections, which will be discussed in section 8.

4. Other hardware

Gradient-echo EPI, the most common acquisition method for fMRI, is sensitive to magnetic susceptibility, which results in signal dephasing and local distortions as well as BOLD sensitivity (Deichmann et al., 2002). Hence, the high SNR and BOLD sensitivity at high field are accompanied by increased distortions. Higher-order shimming is now routinely used to reduce susceptibility effects, though distortions and dropout are typically still evident in the inferior part of the brain. In 2D EPI, decreasing the slice thickness further reduces through-plane dephasing (Deichmann et al., 2002; Wald, 2012). Distortion and blurring can be reduced with the careful manipulation of phase-encoding directions depending on the intended usage (e.g. in the L-R direction to minimize the Field-of-View in the phase-encoding direction, as was done in the Human Connectome Project (Smith et al., 2013)). Respiration or participant motion may additionally alter the B0 homogeneity during the scan and induce dynamic dephasing and distortions as well as spin history effects (Yancey et al., 2011). These can bias functional connectivity metrics towards short-distance correlations in resting state (Van Dijk et al., 2012). Online tracking of B0 with field cameras (Fillmer et al., 2016) or navigators (Wallace et al., 2021), and a dynamic update of the shim can reduce distortions, improve temporal signal to noise ratio (tSNR) (Wallace et al., 2021) and result in robust resting-state network correlations (Fillmer et al., 2016). Motion can be further mitigated with head molds (Power et al., 2019) or with prospective motion correction approaches to naturally complement dynamic B0-shimming. Prospective motion correction approaches based on camera trackers or

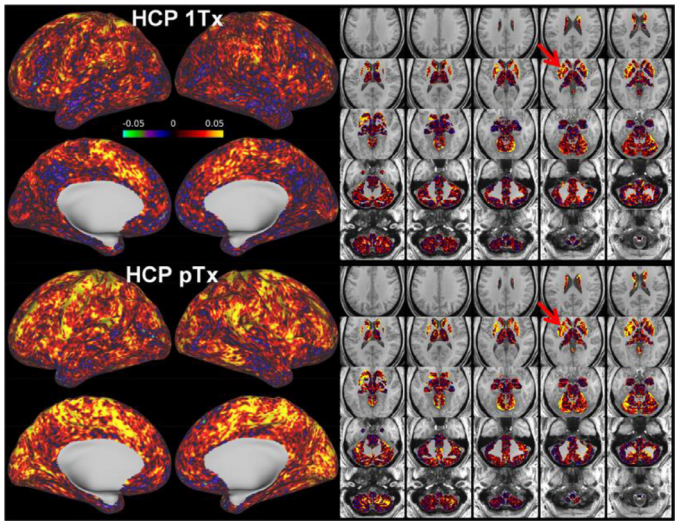

Fig. 2. Seed-based dense connectome with a Human Connectome-like protocol at 7 T (seed in putamen as highlighted by a red arrow). Top, single transmit coil with dielectric pads. Bottom, 8 transmit coil with pTX multiband pulses. The pTX protocol shows stronger functional connectivity between the seed and the rest of the brain especially the cortical regions, as a result of improved flip angle homogeneity. Figure adapted from (Wu et al., 2019).

motion estimates from the fMRI data itself have been shown to reduce the negative correlation between motion and BOLD (e.g. due to signal dropouts), increase tSNR and resting-state sensitivity, particularly for slower, higher-resolution acquisitions (Huang et al., 2018; Lanka and Deshpande, 2019; Maziero et al., 2020; Zaitsev et al., 2017).

Besides B0 inhomogeneity, B1 tends to destructively interfere at higher fields (Vaidya et al., 2016). This is particularly an issue for high-flip angle techniques, but can also decrease BOLD functional connectivity in resting state (e.g. with a typical Human Connectome protocol, see Fig. 2 (Wu et al., 2019)). RF homogeneity can be passively improved with the usage of dielectric pads (Yang et al., 2006), as was done for the 7T fMRI acquisitions of the Human Connectome project (Smith et al., 2013), or with the combination of parallel RF transmit (pTX) either statically (i.e. by calculating an individual- and channel-specific phase or amplitude offset to optimize B1 homogeneity) or dynamically (for example by further modulating the RF for each slice in a SMS protocol) (Deniz, 2019). Such RF optimizations can be time-consuming, but have been shown to be robust between individuals, so that non-individual-specific weightings still result in good excitation homogeneity (Gras et al., 2017) and produce BOLD functional connectivity gains (Wu et al., 2019). pTX further naturally lends itself to the so-called zoomed-EPI approaches that allow very fast fMRI acquisition (Feinberg and Yacoub, 2012; van der Zwaag et al., 2018). pTX is becom-

ing less expensive and better supported by scanner vendors and may become the norm for ultra-high field fMRI in the future (Gras et al., 2019). For fMRI techniques such as ASL and VASO that depend on longitudinal inversion, adiabatic pulses are also now commonly used due to their insensitivity to B1 inhomogeneity (Bause et al., 2016; Huber et al., 2018; Ivanov et al., 2017).

Most of the gains in fMRI sampling rate and image quality are due to the development of receive arrays with multiple smaller receive elements in a 3D arrangement. Smaller receives show higher SNR (Kumar et al., 2009; Roemer et al., 1990) with improvements in fMRI sensitivity (Petridou et al., 2013; Priovoulos et al., 2021). Crucially, the multiple receivers constitute an additional spatial-encoding mechanism due to their differential sensitivity fields (an effect accentuated at higher field). This permits extensive undersampling of the k-space, thus allowing fast volume acquisitions, high spatial-resolution and reduced susceptibility artifacts in fMRI. Parallel imaging techniques have been shown to produce resting state networks with higher sensitivity or in less scanning time (Anteraper et al., 2013; Narsude et al., 2014; Preibisch et al., 2015; Salomon et al., 2014; Smitha et al., 2018) leading to the development of even higher count receive arrays (Hendriks et al., 2020; Wiggins et al., 2009). Note that the intrinsic SNR gains of these arrays are largely in the periphery of the brain, but due to their improved parallel imaging performance (e.g. in SENSE techniques) they also tend to show better SNR in the center of the brain with high-acceleration acquisitions (Bollmann and Barth, 2020; Wald, 2012). fMRI improvements are further fueled by the successful integration of high-amplitude and slew-rate gradients (for example, the Human Connectome project used a gradient coil capable of producing fields up to 300 mT/m with 200 T/m/s (McNab et al., 2013; Wald, 2012)). High-performance gradients are critical for the usage of advanced multiband pulses for highly-accelerated imaging (Barth et al., 2016) and further allow a shorter echo spacing, thus resulting in reduced distortions and drop-out in the EPI image (Tan et al., 2016). The current limitations on gradient performance are largely set by the peripheral nervous stimulation that the fast-slewing gradients induce, rather than by hardware limitations. Dedicated head-only gradient coils or physiological modeling may reduce nervous stimulation further in the future and allow the usage of even stronger/faster gradients (Davids et al., 2019; Wong, 2012).

5. Fast fMRI

Aided by the advent of parallel imaging, fast fMRI is increasingly prevalent in resting state studies, despite the hemodynamic response being relatively sluggish. At low sampling rates, physiological noise from respiration and cardiac pulsation aliases to the lower, brain function-relevant frequency bands (Chen et al., 2020). This physiological effect is particularly critical in resting state, since there is no assumption of a task timeseries. Increasing the sampling rate can reduce the spectral overlap of these physiological processes on resting state (Huotari et al., 2019) and/or facilitate the removal of structured noise from fMRI timeseries (Agrawal et al., 2020). Fast fMRI can also allow us to examine how brain function at rest relates to other processes such as cardiac pulsation and respiration (Jacobs et al., 2020; Napadow et al., 2008; Wu and Marinazzo, 2016) or CSF flow (Fultz et al., 2019). The faster readouts can increase the sensitivity of multivariate approaches (Demetriou et al., 2018) and potentially achieve the same sensitivity in less time in the scanner, which is important for clinical populations (Preibisch et al., 2015), though this is still controversial (Akin et al., 2017; Chen et al., 2019; Demetriou et al., 2018; Huotari et al., 2019). Furthermore, while most of the power of the resting state BOLD fluctuations is in the slower 0.01–0.1 Hz band, higher frequencies may also hold brain function-relevant information that may be interesting to sample (Gohel and Biswal, 2015). Finally, there is an ongoing discussion about the stationarity characteristics of fMRI resting state timeseries (Dai et al., 2016; Jones et al., 2012; , but fast fMRI has provided evidence for distinct brain connectivity states that change dynamically, a phenomenon that is gathering increasing attention (Preti et al., 2016; Zalesky et al., 2014).

As noted in section 4, fast fMRI was popularized with the advent of multiple-receiver coils, that allow the unfolding of simultaneously-acquired but spatially-distinct data through the differential spatial sensitivity profiles of the receivers. While several techniques have been developed, the two most popular are the Multiband (or Simultaneous Multislice) and 3D-EPI. Multiband imaging has probably experienced the widest uptake of all methods mentioned here, greatly benefitting from the development and distribution by the Human Connectome Project. Multiband pulses excite several slices simultaneously that can then be unfolded, providing that there are enough distinct receives per unit distance (Barth et al., 2016). The typical number of simultaneously-excited slices is MB2-4 (Multiband factor), up to MB8 for the popular CMRR protocol of the Human Connectome project (Moeller et al., 2010; Smith et al., 2013), thus allowing an equally reduced TR and potentially improved network detection and shorter scan times (Preibisch et al., 2015; Smitha et al., 2018). When the multiband factor is increased beyond the decoding capabilities of the rf-coil, signal leakage between slices may occur (Todd et al., 2016). However, the multiband factor, and fMRI sampling rate, can be further increased if the overlap between slices is artificially minimized with approaches like CAIPIRINHA (Breuer et al., 2005; Setsompop et al., 2012). The acquisition can additionally be accelerated by combining with other sparse-sampling schemes, such as partial Fourier, to reduce the TR and potentially the echo time (Feinberg et al., 1986). Nowadays, fast online reconstructions are available from all major vendors, greatly simplifying workflows and data handling. One aspect to take into account for high temporal resolution data is that the conventional auto-correlation models might not be sufficient for data acquired with faster TRs (Bollmann et al., 2018). Higher-degree temporal autocorrelation models are advised for task-related GLM fast fMRI, but they may be beneficial also in resting-state analysis, for example when fitting nuisance regressors (Bright et al., 2017).

In 3D-EPI, the slice direction is also defined with a phase encoding gradient. As the entire imaging volume is excited every TR, much smaller flip angles are used, which can be an advantage over the more SAR-intensive multiband pulses. The second phase encoding gradient also means that the acquisition can be accelerated in the slab-direction, while keeping the echo time and BOLD contrast constant (Poser et al., 2010). This feature has been used to achieve very high spatial resolution (Batson et al., 2015). A 2D-CAIPIRINHA scheme can also be used here to permit higher acceleration factors (Narsude et al., 2016). The biggest difference between 3D-EPI and multiband 2D-EPI is the sensitivity to physiological noise (in 3D-EPI) and spin-history artefacts (in MB-EPI). The longer effective averaging time in 3D-EPI leads to both higher SNR and higher sensitivity to system instabilities, including physiological noise (van der Zwaag et al., 2012). At moderate spatiotemporal resolutions, this necessitates physiological noise removal (Jorge et al., 2013). However, in faster acquisitions, with a volume TR of ~0.5 s, 3D-EPI and multiband are equivalent in terms of detection of resting state networks (Reynaud et al., 2017). When profiting from the volumetric acquisition to introduce fast water excitation and elliptical sampling, 3D-EPI was found to outperform a matched MB-EPI sequence (Stirnberg et al., 2017).

Even faster approaches include the Magnetic Resonance Electroencephalography (MREG). In its typical implementation, MREG traverses the k-space in a stack-of-spirals trajectory (Zahneisen et al., 2012). This allows for extensive undersampling and a subsequent whole-brain acquisition at < 100 ms at low spatial resolutions (e.g. a nominal spatial resolution of $3 \times 3 \times 3$ mm^3) (Hennig et al., 2020). This has allowed the detection of resting state networks at frequencies above 0.1 Hz (Akin et al., 2017), improved individual level network detection (Lee et al., 2013) as well as the extraction of resting-state networks from sub-minute fMRI segments, thus greatly facilitating dynamic functional connectivity analyses (Akin et al., 2017; Jacobs et al., 2014). A draw-

back, besides the limited spatial resolution, is the computationally intensive reconstruction.

Similar to the MREG, inverse imaging (InI) increases the sampling rate of traditional functional MRI due to the minimal time required to traverse k-space, at a cost of a moderate reduction in spatial resolution (Lin et al., 2012). InI derives spatial information by solving inverse problems using data simultaneously acquired from all channels in the array, leading to whole-brain coverage at ~100 ms and 5 mm spatial resolution. The spectral characteristics of resting state networks with generalized inverse imaging (GIN) have been investigated by Boyacioglu at al. (Boyacioglu et al., 2013) with 50 ms TR and 3.5 mm isotropic resolution.

Keyhole techniques also allow significantly improved temporal resolution (Gao et al., 1996), while keeping the same spatial resolution. A combination of the keyhole concept with EPI sequences (EPIK) (Zaitsev et al., 2001), has proven to be more robust against susceptibility and chemical-shift artifacts than single-shot EPI. The performance of EPIK, in term of BOLD sensitivity and functional connectivity, has been evaluated by Yun at al. (Yun et al., 2019) through a visually-guided finger-tapping task.

These acquisition advances promise that fast fMRI will become a mainstay of rs-fMRI, with increasing usage. To further establish fast imaging, dedicated data processing may be beneficial, such as avoiding the typically-applied low-pass filter that removes statistical degrees-of-freedom and may insert high-frequency noise (Chen et al., 2019) and accounting for the higher-degree temporal autocorrelation where relevant (Agrawal et al., 2020; Bright et al., 2017).

6. Multi-echo fMRI and connectomics

Multi-echo fMRI acquisition is an extension of the standard 2D BOLD EPI, which involves acquisition of images at multiple TEs instead of only one (Kundu et al., 2012; Poser et al., 2006; Posse, 2012). The use of multi-echo fMRI in the study of connectomics has emerged as a strategy for contending with artifacts from head motion, imaging, and non-neuronal physiology in fMRI datasets. Having signal time series at multiple echo times (TEs), enables evaluation of both BOLD contrast dynamics and time series activity concurrently (Bright and Murphy, 2013; Buur et al., 2009; Kundu et al., 2012). The advantages of the multi-echo fMRI approach are most evident when assumptions regarding BOLD contrast and time series dynamics deviate from ideal conditions, which occurs when imaging patients, at high-field and deep brain regions (Kundu et al., 2017). In these cases, multi-echo fMRI can separate BOLD signal from artifacts in the time series (Peltier and Noll, 2002). Specifically, BOLD percent signal changes scale linearly with TE, whereas artifactual signals from hardware instabilities, motion, or physiology do not exhibit this dependence, and are thus TE-independent.

Nevertheless, the advantages of ME-fMRI are largest when data is acquired at moderate spatial resolution and at low to moderate field strength, on a system with high-performing gradients. If these ingredients are not present, sampling multiple echoes before TE=T2* can only be achieved with detrimentally high acceleration factors, which counteracts the benefits of acquiring multiple echoes (de Hollander et al., 2017; Harms et al., 2018).

Hence, typical multi-echo fMRI acquisition parameters at 3.0 T involve voxel sizes from 2.0 mm to 3.5 mm isotropic, R=2 to 3 in-plane acceleration, three to five TEs usually spanning ~10–60 ms, and TR ranging from 800 ms to 3.0 s with and without multi-band acceleration.

Reconstructing multi-echo fMRI results in separate 3D+time datasets corresponding to the different acquired TEs. Combining the separate 4D datasets into a single time series through averaging with BOLD-sensitive weights has been shown as a reliable means of mitigating susceptibility artifacts, increasing BOLD contrast, and reducing thermal noise across the brain volume. Implementing a matched filter by averaging with voxel-wise weights based on voxel-wise T2* estimates and TE yields optimum contrast at all voxels by approximating acquisition at TE=T2* at each voxel (Morris et al., 2019; Poser et al., 2006). This enhancement leads to appreciable improvements in resting state fMRI functional connectivity mapping (and task activation) in deep brain regions with low signal amplitude and susceptibility artifacts such as the orbitofrontal cortex and inferior temporal cortex (Dipasquale et al., 2017; Kirilina et al., 2016).

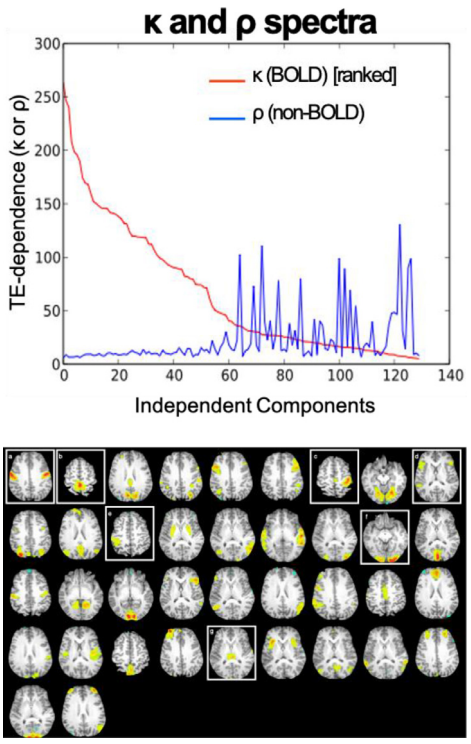

Fig. 3. (*top*) κ and ρ spectra of an individual multi-echo dataset differentiating BOLD and non-BOLD components. (*bottom*) Boxes highlight high- κ components in the motor cortex, hand area of motor cortex, Broca's area network, lateralized sensory cortex, primary visual cortices and thalamic resting state network.

The TE-dependence of linear components of spatiotemporal datasets can also be evaluated. After decomposition of multi-echo datasets with principal component analysis (PCA) or ICA, a weighted average of goodness of fit statistics provides a summary statistic for component-level TE-dependence, κ, and TE-independence, ρ. This strategy is the basis for the analysis and denoising technique called multi-echo independent components analysis (ME-ICA) (Kundu et al., 2012).

Spatial ICA of the dimensionally reduced dataset produces components with κ and ρ values that indicate subsets of component in two separable regimes. The first shows high BOLD weighting (high κ) and low non-BOLD weighting (low ρ), and the second has low κ, and high or low ρ (Fig. 3). Removing components of the low-κ regime by linear projection results in time series denoising of numerous artifacts related to subject head motion, cardiac pulsation, in-plane and through-plane acceleration, and even baseline signal drifts (Power et al., 2018).

The advantages of multi-echo fMRI acquisition and analysis have been demonstrated in a wide range of connectomic studies across field strengths, experimental conditions, and at subject and population levels. Task-based analysis of multi-echo fMRI shows increases in sensitivity to individual events, and with concomitant resting state fMRI, intra- and inter-subject variability of task activation and connectivity patterns is decreased (Gonzalez-Castillo et al., 2016). Resulting increases in statistical power lead to two- to four-fold reductions in required sample size to achieve significant findings in key connectivity patterns, particularly across cortical and subcortical areas and in precision connectomics. (Baek et al., 2017; Lombardo et al., 2016; Lynch et al., 2020; Morris et al., 2016).

Other notable areas of functional neuroscience are also seeing novel applications of ME-ICA, particularly neuropsychopharmacology. A recent study using multi-echo fMRI acquisition at 3 T MRI on the response of patients with major depressive disorder to the recently FDA-approved antidepressant ketamine showed that, after a 40-min infusion, patients had increased functional connectivity between the hippocampus and subgenual anterior cingulate cortex proportional to their performance and activation on the incentive flanker task (Morris et al., 2020).

Because ME-ICA makes no assumptions on the number or characteristics of functional networks in a given dataset, it can be used to study variations in component number with condition. Multi-echo fMRI data acquired in a cohort of healthy volunteers aged 40 to 80 showed a consistent reduction in the number of resting state components 1-hour after emerging from general anesthesia (Nir et al., 2020). A study on multi-echo fMRI across the age range showed an exponential decrease in component number with age from age 8 to 40, alongside increasing functional connectivity in cortical networks (Kundu et al., 2018). The age-dependence of functional connectivity network integration has also been demonstrated in a larger neurodevelopmental study (Váša et al., 2020).

7. Other contrasts

Despite its high sensitivity to deoxyhemoglobin variations and widespread availability, rs-fMRI based on GE has several drawbacks: 1.) The spatial specificity is limited, as the BOLD signal is predominantly driven by the large draining vessels. 2.) Images contain geometric distortions because of the long EPI readout and are sensitive to signal dropout in regions near air cavities. 3.) BOLD signal does not provide a direct or quantitative measure of brain function.

7.1. SE-EPI

Although less sensitive, spin-echo EPI (SE-EPI) can also be used for BOLD imaging, with the advantage of an increased localization of the neuronal activity (Koopmans et al., 2012; Norris, 2012) and higher robustness against signal dropouts (Boyacioğlu et al., 2014; Chiacchiaretta and Ferretti, 2015; Khatamian et al., 2016; Norris, 2012). The benefit of conducting an fMRI experiment with SE at 3T is usually low, as the gain in specificity is not that large, susceptibility-induced distortions remain and the sensitivity loss in some regions is quite high (Koopmans et al., 2012; Norris, 2012). Nevertheless, two studies showed that SE-EPI based rs-fMRI at 3T provides higher sensitivity, specificity, and inter-subject reproducibility in high-susceptibility regions (Chiacchiaretta and Ferretti, 2015; Khatamian et al., 2016) and see Fig. 4.

High spatial resolution is easier at high field (see section 3), but there are fundamental difficulties for SE BOLD data acquisition at 7T. First, the TE needs to match the longer gray matter T2, rather than the T2*, making it challenging to acquire whole-brain data quickly. Another problem is SAR deposition because of the refocusing pulse (see section 4 and (Poser and Norris, 2007)). Although challenging, the 7T implementation of SE-EPI with PINS is a compelling alternative because it can achieve fair spatial and temporal resolution (Koopmans et al., 2012). Nevertheless, the sensitivity penalties are high, the requirements for this implementation are challenging, and the sequence is not yet widely available.

7.2. ASL-CBF

With recent technical advances, Arterial Spin Labeling (ASL) is gradually becoming a more feasible alternative to BOLD fMRI (Borogovac and Asllani, 2012; Chen et al., 2015; Vidorreta et al., 2013). ASL is a non-invasive method that uses the water present in the arterial blood as a freely diffusible intrinsic tracer to measure tissue perfusion. Quantitative CBF maps can be obtained using Buxton's General Kinetic Model (Buxton et al., 1998). Similar to BOLD rs-fMRI, functional ASL experiments are performed with a timeseries acquisition where a pairwise acquisition (label-control) is acquired (Borogovac and Asllani, 2012).

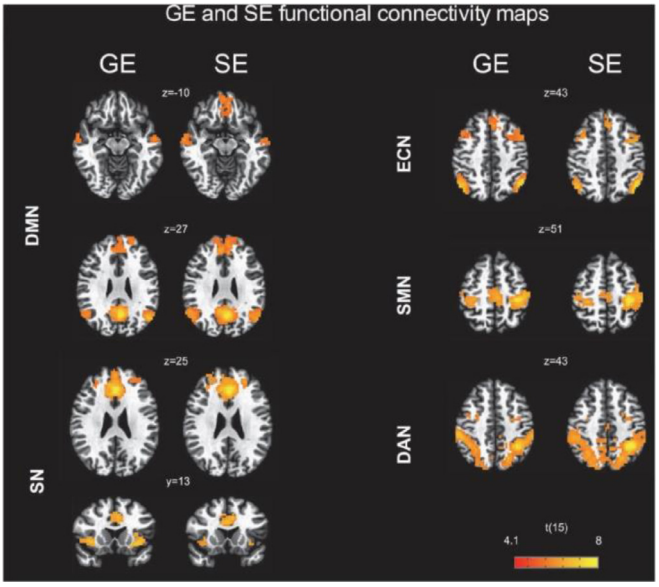

Fig. 4. GE and SE functional connectivity maps. A seed-based connectivity map for Gradient echo (GE) and Spin echo (SE) obtained from random effects group analysis showing the following resting state networks: default mode network (DMN), executive control network (ECN), salience network (SN), dorsal attention network (DAN), sensorimotor network (SMN). Differences are especially large in the inferior frontal areas of the DMN. Figure adapted from (Chiacchiaretta and Ferretti, 2015).

There are several possible labelling implementation schemes for ASL. Due to its straightforward implementation and relatively high SNR, pseudocontinuous (pCASL) labelling has become the method of choice for most ASL experiments (Alsop et al., 2015). Although the typical readout is 2D GE EPI, the timing differences between slices mean that for a whole-brain resting state connectivity measurement, 3D acquisitions are usually preferable. BOLD contamination can be quite pronounced because of the GE-EPI readout. Hence, a 3D Gradient and Spin-Echo (GRASE) readout (Günther et al., 2005) emerged as an alternative to the 2D readout (Liang et al., 2012), providing higher SNR and more brain coverage. The 3D GRASE acquisition, in combination with pCASL and Background Suppression (BS) (Garcia et al., 2005) seems to be the current optimal protocol for both static and dynamic resting state ASL, though it is not yet widely available (Alsop et al., 2015; Chen et al., 2015). Another motivation for an ASL acquisition at high field is the prolonged blood T1, which can amplify the perfusion signal. There are not many ASL fMRI experiments at 7T but an interesting study employed Turbo-Flash (Fast Low Angle Shot) ASL (both pCASL and PASL) and showed its feasibility in a 7T resting state experiment (Zuo et al., 2013).

Compared to GE-EPI, ASL offers a direct and quantifiable CBF measure, and increased spatial specificity to neuronal activity due to the capillary signal origin of ASL. The main drawbacks of ASL are its intrinsic low signal-to-noise ratio (SNR), and the temporal resolution, which is usually much lower than BOLD GE rs-fMRI protocols. Despite its disadvantages, ASL has gained considerable attention. Several studies demonstrated the viability of characterizing intrinsic brain activity with ASL maps (Biswal et al., 1997; Chen et al., 2015; Jann et al., 2015; Liang et al., 2014; Viviani et al., 2011). The recently improved post-processing methods for subtraction and filtering have also contributed to the rising number of resting-state functional connectivity studies using ASL (Chuang et al., 2008; Jann et al., 2016; Liang et al., 2015; Silva et al., 2018; Wang et al., 2008).

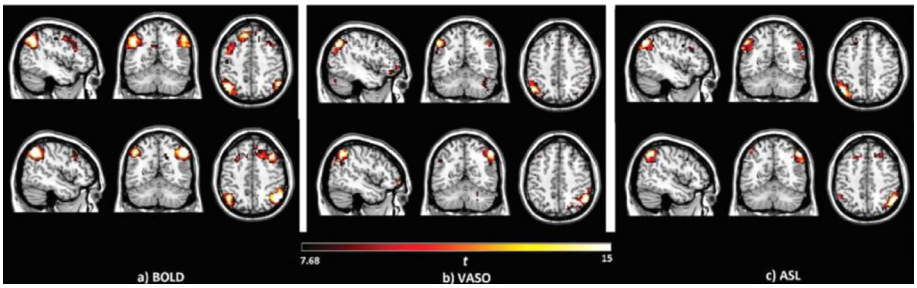

Fig. 5. Left/Right executive control networks identified with a seed-based analysis of the A) blood oxygen level dependent (BOLD), B) vascular space occupancy (VASO) and C) Arterial Spin Labeling (ASL) data. Figure adapted from (Zhang et al., 2018).

ASL has been used as an alternative to rs-BOLD in several clinical investigations in Schizophrenia (Kindler et al., 2015; Oliveira et al., 2018; Zhu et al., 2015), chronic fatigue (Boissoneault et al., 2016), epilepsy (Boscolo Galazzo et al., 2019; Xu et al., 2021), healthy ageing (Galiano et al., 2020) and psychosis (Overton et al., 2020). Recent studies show that ASL provides enough statistical power, reproducibility and low-frequency variations comparable to BOLD (Federspiel et al., 2006; Jann et al., 2015), but it is still limited by partial brain coverage in the majority of the sequences used.

7.3. VASO-CBV

Similarly, spontaneous fluctuation in CBV-weighted signal can also be used for resting state functional connectivity (Huber et al., 2017, 2020; Miao et al., 2014; Zhang et al., 2018). The Vascular Space Occupancy (VASO) sequence takes advantage of the T1 differences between blood and the surrounding tissue to null blood signal and measure CBV changes (Lu et al., 2003). Recently, VASO fMRI gained attention because it offers higher spatial specificity than GE BOLD (Huber et al., 2015; Jin and Kim, 2008). Similar to ASL, much smaller coverage is achieved in VASO than in BOLD fMRI experiments. Also, VASO is less sensitive than GE BOLD fMRI (Oliveira et al., 2021).

The first study that showed VASO-CBV resting-state functional connectivity was conducted by Miao et al. 2014 (Miao et al., 2014), using a 3T scanner. For a whole-brain acquisition, a single-shot 3D GRASE readout was used (Poser and Norris, 2009), which also yields increased SNR, minimum BOLD contamination and low sensitivity to susceptibility artefacts. Their functional connectivity analysis consisted of a thorough comparison between VASO-CBV and BOLD using ICA and seed-based analysis, identifying the DMN, salience-, executive control-, visual-, auditory-, and sensorimotor networks.

Another exciting study was published by Zhang et al. 2018, comparing GE BOLD, CBF and CBV resting-state functional connectivity metrics within the same group of subjects using a seed-based approach. Both VASO and ASL were more specific and less sensitive than GE-BOLD (Fig. 5). These differences are at least partially biologically driven (Zhang et al., 2018).

A recent VASO variant was used for resting state connectivity analysis at high spatial resolution (< 1 mm) in a small slab covering M1 (Huber et al., 2017) and will be described in section 8 below. A Slice Selective Slab Inversion VASO (Huber et al., 2014) was employed to acquire VASO-CBV and BOLD simultaneously using an interleaved acquisition. Recent technical improvements with Multiple Acquisitions with Global Excitation Cycling (MAGEC) (Huber et al., 2020) allow whole-brain coverage and detection of a larger number of networks.

8. Laminar connectivity

Ultra-high magnetic fields open up novel avenues in the mapping of functional specialization and the flow of information between and across the cortex (Dumoulin et al., 2018; Petridou and Siero, 2019). The thickness of the human cerebral cortex ranges from 1 to 4 mm (Fischl and Dale, 2000) and is highly convoluted. As we cannot distinguish the six layers of the neocortical microcircuit (Felleman and Van Essen, 1991), the BOLD signals are typically described in terms of cortical depth (Dumoulin et al., 2018), which relates loosely to the different cortical layers: feedforward projections arrive in the granular layer (L4), feedback projections terminate in the more superficial supragranular layer (L2/3) and the deeper infragranular (L5/6), while lateral fibers target all areas (Felleman and Van Essen, 1991). Increasing the spatial resolution results in more accurate sampling of the signals arising across depth (Kay et al., 2019). In other words, a conventional 3T fMRI protocol with a voxel dimension of 3 mm practically samples 2 "layers" of the cortex, rendering interpretability at mesoscopic level pointless due to partial voluming; signals from multiple layers/sources are sampled as one (Guidi et al., 2020; Huber et al., 2015). With sub-millimeter fMRI, multiple cortical depths can be separated (Polimeni et al., 2010).

While promising, high-resolution (sub-millimeter) laminar fMRI also faces challenges (Dumoulin et al., 2018). The cortical vascular architecture poses a difficulty for the interpretation of the BOLD signal across depth, as BOLD signal originates primarily from field distortions resulting from deoxygenated blood draining via venules and intracortical veins to larger pial veins at the cortical surface (Kashyap et al., 2018; Turner, 2002; van Dijk et al., 2020). While this problem is inherent to the GE-BOLD-contrast, its consequence is magnified while interpreting signals across depth (Polimeni et al., 2010; Uludağ and Blinder, 2018). The vascular architecture means that venous blood from deeper layers contributes to the BOLD signal in upper layers as it flows towards the pial surface (Heinzle et al., 2016; van Dijk et al., 2020). Advanced modeling strategies capturing the contribution of venous effects (Heinzle et al., 2016; Kay et al., 2020; Markuerkiaga et al., 2016; Marquardt et al., 2018; van Dijk et al., 2020) might enhance interpretability of laminar signals (Larkum et al., 2018). Given that extravascular contamination from the veins at the pial surface decreases rapidly away from the cortical surface (Ogawa et al., 1993) and signals from central layers can be distinguished from those of pial veins (Fracasso et al., 2018), issues inherent to GE-BOLD at the laminar level can, to some extent, be mitigated.

Recognizing these challenges, efforts to map connectivity using resting-state fMRI across and between layers and to develop analysis-strategies are only slowly appearing (Egbert et al., 2021; Guidi et al., 2020; Huber et al., 2020; Shamir and Assaf, 2020). One of the most prominent examples of laminar rs-fMRI with seed-based connectivity showed that the primary motor area (M1) received somatosensory and premotor input in superficial layers and cortico-spinal motor output in deep layers using a slab-selective VASO contrast with 0.75 mm isotropic resolution (Huber et al., 2017). Though challenging, the feasibility of probing laminar connectivity with gradient-echo approaches is increasingly being recognized (Pais-Roldán et al., 2020); using a TR-external GE-EPI with keyhole (EPIK) sequence with 0.63 mm isotropic resolution, Pais et al. were able to show that during rest, the superficial layers show high coherence (a measure of "similarity in frequency content", rather than "correlation in the time domain", thought to be less affected by draining vein effects (Pais-Roldán et al., 2020)). The scope of laminar connectivity has also been broadened towards task-related processes. Depth-dependent connectivity patterns were observed dur-

Table 1
Common resting state fMRI acquisition approaches for different study's goals.

Application	Magnetic Field	Spatial Information	Acquisition Approach	Subject's Condition
Large groups of patients, single-center study	3T	Whole brain coverage (14cm) moderate spatial resolution (2-3mm) Cerebrum coverage Spatial resolution (3-4mm); quantitative CBF also acquired	Multiband EPI or 3D-EPI, TR_{acq} sub-second 2D pCASL EPI TR_{acq} 3–5 s (use ASL for qCBF & connectivity)	Eyes open, fixation cross
Large groups of patients, multi-center study	3T	Whole brain coverage (14 cm) moderate spatial resolution (2-3mm)	2D-EPI, TR_{acq} 2–3 s to avoid differences between vendors	Eyes closed
Individual subject or moderately powered patient studies OR: Seed-based analysis of subcortical structures	3T, 7T	Whole brain coverage (14 cm) moderate spatial resolution (2-3mm)	Multi-echo EPI, 3-4 TEs, TR_{acq}=2.5 s (single-band) TR_{acq}=1.0 s (multi-band); ME-ICA	Eyes open, fixation cross
Changes within a network upon task-related activation	7T	Coverage of network of interest, higher spatial resolution (1.5 mm)	Multiband EPI or 3D-EPI, TR_{acq} ~2 s	Eyes open, fixation cross/ task
Connectivity within layers of a specific gray matter area	7T	Coverage of area of interest Sub-millimeter resolution (0.7–0.8 mm)	VASO with TR_{acq} 3 s or T2*-w 3D-EPI, TR_{acq} ~2 s	Eyes open, fixation cross

ing motor (Pais-Roldán et al., 2020) [0.63 mm isotropic], language [0.943 × 0.9 mm] (Sharoh et al., 2019), and auditory [1.5 mm isotropic] (Wu et al., 2018) processing; all showing the contribution of deeper layers to task performance using a GE-EPI acquisition scheme. These early studies highlight the impact of laminar connectivity, adding an additional dimension to our understanding of the brain using non-invasive methods (Huber et al., 2020).

9. White matter

Although the overwhelming majority of connectivity studies are targeting gray matter networks, there is a recent interest in white matter functional connectivity based on resting state BOLD data. These signals are much smaller than those in gray matter, as both the blood flow (Van Osch et al., 2009) and blood volume (Jensen et al., 2006) are much lower in white matter than in gray matter. Hence, reports of BOLD responses in white matter are relatively rare. The existing literature of task-based responses is mostly focused on the large white matter bundles in the corpus callosum (Gawryluk et al., 2014). Nevertheless, the signal fluctuations found in the white matter in resting state data do show consistent networks (Gore et al., 2019). These networks can be found with similar analysis approaches as used to identify the cortical resting state networks, such as ICA or clustering approaches (Ding et al., 2016; Marussich et al., 2017) and white matter voxels have been shown to contribute at least a little to brain-wide networks (Li et al., 2020).

In terms of acquisition, the same T2* weighted EPI images are acquired for white matter network identification as for cortical resting state analysis. Images tend to be acquired at 3T with a modest spatial resolution of 3.5 mm and TE of ~T2*. For the post-processing, a masking step is added to remove the gray matter, so as to avoid signal swamping from the large BOLD responses. This suffices to make the further post-processing analysis sensitive to the signal correlations in the white matter networks.

In 2016, Ding et al. (2016) showed that the resting state connectivity found in white matter is indeed BOLD-like and TE-dependent, and, hence, separate from physiological effects that are S0-based (Kundu et al., 2012). The same group showed that a hemodynamic response function, HRF, can be derived for white matter (Wang et al., 2020). This white matter HRF has a reduced peak amplitude and delayed peak times compared to the gray matter HRF.

These findings have recently led to the publication of a few papers specifically investigating white matter resting state connectivity, for example observing differences in these networks during baseline or movie watching (Marussich et al., 2017) or differences in clinical populations, such as patients suffering from epilepsy (Jiang et al., 2019) and mild cognitive impairment (Lin et al., 2020).

10. Conclusions

In this review, we presented the most common and recent approaches for different resting state studies, specifically focusing on acquisitions and hardware improvements. In each section, applications have been discussed, to show the potential of rs-fMRI and its growing availability and usage for both fundamental neuroscience and clinical investigations.

In Table 1, we summarize the most common approaches in terms of imaging sequence, spatial and temporal resolution, required field strength and subject behavior, for different purposes, depending on which subject population or specific brain activity is the object of the study.

Overall, we can conclude that lower field strength (3T) is more suitable for large patient studies, where whole brain coverage is required, while extremely high spatial resolution is not essential. For this kind of investigations, multi-band or 3D EPI methods can be used, with a sub-second acquisition time, as well as 2D EPI or 2D pCASL EPI, with TR_{acq} ranging from 3 to 5 s. For most of these applications, subjects are instructed to keep their eyes open and fixate on a fixation cross, except for multi-center studies, where eyes close condition is best to avoid differences in stimulus displays.

Instead, when specific brain regions are targeted (such as when studying deep gray matter, or connectivity within layers for a certain gray matter area), higher field strengths or alternative acquisitions (ME-EPI, VASO/ASL) are more suitable. 7T is essential to reach sub-millimeter spatial resolutions, and this is usually combined with smaller brain coverage.

In conclusion, the exact acquisition parameters will depend on the objective of the study at hand. Nevertheless, this review and Table 1 can guide the new rs-fMRI user to make an informed choice from the possible acquisition schemes currently available for rs-fMRI for functional connectomics.

Credit authorship contribution statement

Luisa Raimondo: Writing – original draft, Writing – review & editing. **Ícaro A.F. Oliveira:** Writing – original draft, Writing – review & editing. **Jurjen Heij:** Writing – original draft, Writing – review & editing. **Nikos Priovoulos:** Writing – original draft, Writing – review & editing. **Prantik Kundu:** Writing – original draft, Writing – review & editing. **Renata Ferranti Leoni:** Writing – original draft, Writing – review & editing. **Wietske van der Zwaag:** Writing – original draft, Writing – review & editing.

Acknowledgements

This work was supported by a Netherlands Organization for Scientific Research (NWO) Vidi Grant (TTW VI.Vidi.198.016 to W.Z.) and a Royal Netherlands Academy for Arts and Sciences (KNAW) Onderzoeksfonds grant (2018 to W.Z and others)

Data and Code Availability Statement

Data for this review paper formed the available literature on resting state functional MRI. We retrieved these through public databases (scopus, web of science, google scholar, pubmed) or directly from the publishers website. All relevant papers are listed in the reference section of the review.

For the writing of this review paper, no code was used.

References

Agcaoglu, O., Wilson, T.W., Wang, Y.P., Stephen, J., Calhoun, V.D., 2019. Resting state connectivity differences in eyes open versus eyes closed conditions. Hum. Brain Mapp. 40, 2488–2498. doi:10.1002/hbm.24539.

Agcaoglu, O., Wilson, T.W., Wang, Y.P., Stephen, J.M., Calhoun, V.D., 2020. Dynamic resting-state connectivity differences in eyes open versus eyes closed conditions. Brain Connect. 10, 504–519. doi:10.1089/brain.2020.0768.

Agrawal, U., Brown, E.N., Lewis, L.D., 2020. Model-based physiological noise removal in fast fMRI. Neuroimage 205, 116231. doi:10.1016/j.neuroimage.2019.116231.

Akin, B., Lee, H.L., Hennig, J., LeVan, P., 2017. Enhanced subject-specific resting-state network detection and extraction with fast fMRI. Hum. Brain Mapp. 38, 817–830. doi:10.1002/hbm.23420.

Alsop, D.C., Detre, J.A., Golay, X., Günther, M., Hendrikse, J., Hernandez-Garcia, L., Lu, H., Macintosh, B.J., Parkes, L.M., Smits, M., Van Osch, M.J.P., Wang, D.J.J., Wong, E.C., Zaharchuk, G., 2015. Recommended implementation of arterial spin-labeled Perfusion mri for clinical applications: a consensus of the ISMRM Perfusion Study group and the European consortium for ASL in dementia. Magn. Reson. Med. 73, 102–116. doi:10.1002/mrm.25197.

Anteraper, S.A., Whitfield-Gabrieli, S., Keil, B., Shannon, S., Gabrieli, J.D., Triantafyllou, C., 2013. Exploring functional connectivity networks with multichannel brain array coils. Brain Connect. 3, 302–315. doi:10.1089/brain.2012.0113.

Baek, K., Morris, L.S., Kundu, P., Voon, V., 2017. Disrupted resting-state brain network properties in obesity: decreased global and putaminal cortico-striatal network efficiency. Psychol. Med. 47, 585–596. doi:10.1017/S0033291716002646.

Barth, M., Breuer, F., Koopmans, P.J., Norris, D.G., Poser, B.A., 2016. Simultaneous multislice (SMS) imaging techniques. Magn. Reson. Med. 75, 63–81. doi:10.1002/mrm.25897.

Batson, M.A., Petridou, N., Klomp, D.W., Frens, M.A., Neggers, S.F., 2015. Single session imaging of cerebellum at 7 Tesla: obtaining structure and function of multiple motor subsystems in individual subjects. PLoS One 10, e0134933. doi:10.1371/journal.pone.0134933.

Bause, J., Ehses, P., Mirkes, C., Shajan, G., Scheffler, K., Pohmann, R., 2016. Quantitative and functional pulsed arterial spin labeling in the human brain at 9.4 T. Magn. Reson. Med. 75, 1054–1063. doi:10.1002/mrm.25671.

Biswal, B., Zerrin Yetkin, F., Haughton, V.M., Hyde, J.S., 1995. Functional connectivity in the motor cortex of resting human brain using echo-planar mri. Magn. Reson. Med. 34, 537–541. doi:10.1002/mrm.1910340409.

Biswal, B.B., Kylen, J.Van, Hyde, J.S., 1997. Simultaneous assessment of flow and BOLD signals in resting-state functional connectivity maps. NMR Biomed. 10, 165–170. doi:10.1002/(SICI)1099-1492(199706/08)10:4/5<165::AID-NBM454>3.0.CO;2-7.

Boissoneault, J., Letzen, J., Lai, S., Robinson, M.E., Staud, R., 2016. Static and dynamic functional connectivity in patients with chronic fatigue syndrome: use of arterial spin labelling fMRI. Clin. Physiol. Funct. Imaging 1–10. doi:10.1111/cpf.12393.

Bollmann, S., Barth, M., 2020. New acquisition techniques and their prospects for the achievable resolution of fMRI. Prog. Neurobiol. 101936. doi:10.1016/j.pneurobio.2020.101936.

Bollmann, S., Puckett, A.M., Cunnington, R., Barth, M., 2018. Serial correlations in single-subject fMRI with sub-second TR. Neuroimage 166, 152–166. doi:10.1016/j.neuroimage.2017.10.043.

Borogovac, A., Asllani, I., 2012. Arterial spin labeling (ASL) fMRI: advantages, theoretical constrains and experimental challenges in neurosciences. Int. J. Biomed. Imaging 2012. doi:10.1155/2012/818456.

Boscolo Galazzo, I., Storti, S.F., Barnes, A., De Blasi, B., De Vita, E., Koepp, M., Duncan, J.S., Groves, A., Pizzini, F.B., Menegaz, G., Fraioli, F., 2019. Arterial spin labeling reveals disrupted brain networks and functional connectivity in drug-resistant temporal epilepsy. Front. Neuroinform. 12, 1–18. doi:10.3389/fninf.2018.00101.

Boyacioglu, R., Beckmann, C.F., Barth, M., 2013. An investigation of RSN frequency spectra using ultra-fast generalized inverse imaging (GIN). Front. Hum. Neurosci. 7, 1–7. doi:10.3389/fnhum.2013.00156.

Boyacioğlu, R., Schulz, J., Müller, N.C.J., Koopmans, P.J., Barth, M., Norris, D.G., 2014. Whole brain, high resolution multiband spin-echo EPI fMRI at 7T: a comparison with gradient-echo EPI using a color-word Stroop task. Neuroimage 97, 142–150. doi:10.1016/j.neuroimage.2014.04.011.

Branco, P., Seixas, D., Castro, S.L., 2018. Temporal reliability of ultra-high field resting-state MRI for single-subject sensorimotor and language mapping. Neuroimage 168, 499–508. doi:10.1016/j.neuroimage.2016.11.029.

Breuer, F.A., Blaimer, M., Heidemann, R.M., Mueller, M.F., Griswold, M.A., Jakob, P.M., 2005. Controlled aliasing in parallel imaging results in higher acceleration (CAIPIRINHA) for multi-slice imaging. Magn. Reson. Med. 53, 684–691. doi:10.1002/mrm.20401.

Bright, M.G., Murphy, K., 2013. Removing motion and physiological artifacts from intrinsic BOLD fluctuations using short echo data. Neuroimage 64, 526–537. doi:10.1016/j.neuroimage.2012.09.043.

Bright, M.G., Tench, C.R., Murphy, K., 2017. Potential pitfalls when denoising resting state fMRI data using nuisance regression. Neuroimage 154, 159–168. doi:10.1016/j.neuroimage.2016.12.027.

Buckner, R.L., Krienen, F.M., Castellanos, A., Diaz, J.C., Thomas Yeo, B.T., 2011. The organization of the human cerebellum estimated by intrinsic functional connectivity. J. Neurophysiol. 106, 2322–2345. doi:10.1152/jn.00339.2011.

Buur, P.F., Poser, B.A., Norris, D.G., 2009. A dual echo approach to removing motion artefacts in fMRI time series. NMR Biomed. 22, 551–560 https://doi.org/10.1002/nbm.1371.

Buxton, R.B., Frank, L.R., Wong, E.C., Siewert, B., Warach, S., Edelman, R.R., 1998. A general kinetic model for quantitative perfusion imaging with arterial spin labeling. Magn. Reson. Med. 40, 383–396. doi:10.1002/mrm.1910400308.

Caparelli, E.C., Ross, T.J., Gu, H., Yang, Y., 2019. Factors affecting detection power of blood oxygen-level dependent signal in resting-state functional magnetic resonance imaging using high-resolution echo-planar imaging. Brain Connect. 9, 638–648. doi:10.1089/brain.2019.0683.

Chen, J.E., Lewis, L.D., Chang, C., Tian, Q., Fultz, N.E., Ohringer, N.A., Rosen, B.R., Polimeni, J.R., 2020. Resting-state "physiological networks. Neuroimage 213, 116707. doi:10.1016/j.neuroimage.2020.116707.

Chen, J.E., Polimeni, J.R., Bollmann, S., Glover, G.H., 2019. On the analysis of rapidly sampled fMRI data. Neuroimage 188, 807–820. doi:10.1016/j.neuroimage.2019.02.008.

Chen, J.J., Jann, K., Wang, D.J.J., 2015. Characterizing resting-state brain function using arterial spin labeling. Brain Connect. 5, 527–542. doi:10.1089/brain.2015.0344.

Chiacchiaretta, P., Ferretti, A., 2015. Resting state BOLD functional connectivity at 3T: spin echo versus gradient echo EPI. PLoS One 10. doi:10.1371/journal.pone.0120398.

Chuang, K.-H., van Gelderen, P., Merkle, H., Bodurka, J., Ikonomidou, V.N., Koretsky, A.P., Duyn, J.H., Talagala, S.L., 2008. Mapping resting-state functional connectivity using perfusion MRI. Neuroimage 40, 1595–1605. doi:10.1016/j.neuroimage.2008.01.006.

Dai, M., Zhang, Z., Srivastava, A., 2016. Testing stationarity of brain functional connectivity using change-point detection in fMRI data. In: 2016 IEEE Conference on Computer Vision and Pattern Recognition Workshops (CVPRW), pp. 981–989. doi:10.1109/CVPRW.2016.126.

Davids, M., Guerin, B., Vom Endt, A., Schad, L.R., Wald, L.L., 2019. Prediction of peripheral nerve stimulation thresholds of MRI gradient coils using coupled electromagnetic and neurodynamic simulations. Magn. Reson. Med. 81, 686–701. doi:10.1002/mrm.27382.

de Hollander, G., Keuken, M.C., van der Zwaag, W., Forstmann, B.U., Trampel, R., 2017. Comparing functional MRI protocols for small, iron-rich basal ganglia nuclei such as the subthalamic nucleus at 7 T and 3 T. Hum. Brain Mapp. 38, 3226–3248 https://doi.org/10.1002/hbm.23586.

De Martino, F., Esposito, F., van de Moortele, P.F., Harel, N., Formisano, E., Goebel, R., Ugurbil, K., Yacoub, E., 2011. Whole brain high-resolution functional imaging at ultra high magnetic fields: an application to the analysis of resting state networks. Neuroimage 57, 1031–1044. doi:10.1016/j.neuroimage.2011.05.008.

Deichmann, R., Josephs, O., Hutton, C., Corfield, D.R., Turner, R., 2002. Compensation of susceptibility-induced BOLD sensitivity losses in echo-planar fMRI imaging. Neuroimage 15, 120–135. doi:10.1006/nimg.2001.0985.

Demetriou, L., Kowalczyk, O.S., Tyson, G., Bello, T., Newbould, R.D., Wall, M.B., 2018. A comprehensive evaluation of increasing temporal resolution with multiband-accelerated protocols and effects on statistical outcome measures in fMRI. Neuroimage 176, 404–416. doi:10.1016/j.neuroimage.2018.05.011.

Deniz, C.M., 2019. Parallel transmission for ultrahigh field MRI. Top. Magn. Reson. Imaging 28, 159–171. doi:10.1097/rmr.0000000000000204.

Ding, Z., Xu, R., Bailey, S.K., Wu, T.L., Morgan, V.L., Cutting, L.E., Anderson, A.W., Gore, J.C., 2016. Visualizing functional pathways in the human brain using correlation tensors and magnetic resonance imaging. Magn. Reson. Imaging 34, 8–17. doi:10.1016/j.mri.2015.10.003.

Dipasquale, O., Sethi, A., Lagan, M.M., Baglio, F., Baselli, G., Kundu, P., Harrison, N.A., Cercignani, M., 2017. Comparing resting state fMRI de-noising approaches using multi-and single-echo acquisitions. PLoS One 12, 1–25. doi:10.1371/journal.pone.0173289.

Donahue, M.J., Hoogduin, H., Smith, S.M., Siero, J.C.W., Chappell, M., Petridou, N., Jezzard, P., Luijten, P.R., Hendrikse, J., 2012. Spontaneous blood oxygenation level-dependent fMRI signal is modulated by behavioral state and correlates with evoked response in sensorimotor cortex: A 7.0-T fMRI study. Hum. Brain Mapp. 33, 511–522. doi:10.1002/hbm.21228.

Dumoulin, S.O., Fracasso, A., van der Zwaag, W., Siero, J.C.W., Petridou, N., 2018. Ultra-high field MRI: advancing systems neuroscience towards mesoscopic human brain function. Neuroimage 168, 345–357. doi:10.1016/j.neuroimage.2017.01.028.

Ebneabbasi, A., Mahdipour, M., Nejati, V., Li, M., Liebe, T., Colic, L., Leutritz, A.L., Vogel, M., Zarei, M., Walter, M., Tahmasian, M., 2020. Emotion processing and regulation in major depressive disorder: a 7T resting-state fMRI study. Hum. Brain Mapp. 797–810. doi:10.1002/hbm.25263.

Egbert, A.R., Lojek, E., Biswal, B., Pluta, A., Harmonia, G., 2021. The laminar pat-

tern of resting state in human cerebral cortex. Magn. Reson. Imaging 76, 8–16. doi:10.1016/j.mri.2020.10.013.
Ertürk, M.A., Raaijmakers, A.J., Adriany, G., Uğurbil, K., Metzger, G.J., 2017. A 16-channel combined loop-dipole transceiver array for 7 Tesla body MRI. Magn. Reson. Med. 77, 884–894. doi:10.1002/mrm.26153.
Federspiel, A., Müller, T.J., Horn, H., Kiefer, C., Strik, W.K., 2006. Comparison of spatial and temporal pattern for fMRI obtained with BOLD and arterial spin labeling. J. Neural Transm. 113, 1403–1415. doi:10.1007/s00702-006-0434-5.
Feinberg, D.A., Hale, J.D., Watts, J.C., Kaufman, L., Mark, A., 1986. Halving MR imaging time by conjugation: demonstration at 3.5 kG. Radiology 161, 527–531. doi:10.1148/radiology.161.2.3763926.
Feinberg, D.A., Yacoub, E., 2012. The rapid development of high speed, resolution and precision in fMRI. Neuroimage 62, 720–725. doi:10.1016/j.neuroimage.2012.01.049.
Felleman, D.J., Van Essen, D.C., 1991. Distributed hierarchical processing in the primate cerebral cortex. Cereb. Cortex 1, 1–47. doi:10.1093/cercor/1.1.1.
Fillmer, A., Vannesjo, S.J., Pavan, M., Scheidegger, M., Pruessmann, K.P., Henning, A., 2016. Fast iterative pre-emphasis calibration method enabling third-order dynamic shim updated fMRI. Magn. Reson. Med. 75, 1119–1131. doi:10.1002/mrm.25695.
Fischl, B., Dale, A.M., 2000. Measuring the thickness of the human cerebral cortex from magnetic resonance images. Proc. Natl. Acad. Sci. USA 97, 11050–11055. doi:10.1073/pnas.200033797.
Fracasso, A., Luijten, P.R., Dumoulin, S.O., Petridou, N., 2018. Laminar imaging of positive and negative BOLD in human visual cortex at 7T. Neuroimage 164, 100–111. doi:10.1016/j.neuroimage.2017.02.038.
Fultz, N.E., Bonmassar, G., Setsompop, K., Stickgold, R.A., Rosen, B.R., Polimeni, J.R., Lewis, L.D., 2019. Coupled electrophysiological, hemodynamic, and cerebrospinal fluid oscillations in human sleep. Science 366 (80-.), 628–631. doi:10.1126/science.aax5440.
Galiano, A., Mengual, E., García de Eulate, R., Galdeano, I., Vidorreta, M., Recio, M., Riverol, M., Zubieta, J.L., Fernández-Seara, M.A., 2020. Coupling of cerebral blood flow and functional connectivity is decreased in healthy aging. Brain Imaging Behav. 14, 436–450. doi:10.1007/s11682-019-00157-w.
Gao, J., Xiong, J., Lai, S., Haacke, E.M., Woldorff, M.G., Li, J., Fox, P.T., 1996. Improving the temporal resolution. Magn. Reson. Med. 35, 854–860.
Garcia, D.M., Duhamel, G., Alsop, D.C., 2005. Efficiency of inversion pulses for background suppressed arterial spin labeling. Magn. Reson. Med. 54, 366–372. doi:10.1002/mrm.20556.
Gawryluk, J.R., Mazerolle, E.L., D'Arcy, R.C.N., 2014. Does functional MRI detect activation in white matter? A review of emerging evidence, issues, and future directions. Front. Neurosci. 8, 1–12. doi:10.3389/fnins.2014.00239.
Gohel, S.R., Biswal, B.B., 2015. Functional integration between brain regions at rest occurs in multiple-frequency bands. Brain Connect. 5, 23–34. doi:10.1089/brain.2013.0210.
Gonzalez-Castillo, J., Panwar, P., Buchanan, L.C., Caballero-Gaudes, C., Handwerker, D.A., Jangraw, D.C., Zachariou, V., Inati, S., Roopchansingh, V., Derbyshire, J.A., Bandettini, P.A., 2016. Evaluation of multi-echo ICA denoising for task based fMRI studies: block designs, rapid event-related designs, and cardiac-gated fMRI. Neuroimage 141, 452–468 https://doi.org/10.1016/j.neuroimage.2016.07.049.
Gore, J.C., Li, M., Gao, Y., Wu, T.L., Schilling, K.G., Huang, Y., Mishra, A., Newton, A.T., Rogers, B.P., Chen, L.M., Anderson, A.W., Ding, Z., 2019. Functional MRI and resting state connectivity in white matter - a mini-review. Magn. Reson. Imaging 63, 1–11. doi:10.1016/j.mri.2019.07.017.
Gras, V., Boland, M., Vignaud, A., Ferrand, G., Amadon, A., Mauconduit, F., Le Bihan, D., Stöcker, T., Boulant, N., 2017. Homogeneous non-selective and slice-selective parallel-transmit excitations at 7 Tesla with universal pulses: a validation study on two commercial RF coils. PLoS One 12, e0183562. doi:10.1371/journal.pone.0183562.
Gras, V., Poser, B.A., Wu, X., Tomi-Tricot, R., Boulant, N., 2019. Optimizing BOLD sensitivity in the 7T human connectome project resting-state fMRI protocol using plug-and-play parallel transmission. Neuroimage 195, 1–10. doi:10.1016/j.neuroimage.2019.03.040.
Guidi, M., Huber, L., Lampe, L., Merola, A., Ihle, K., Moller, H.E., 2020. Cortical laminar resting-state signal fluctuations scale with the hypercapnic blood oxygenation level-dependent response. Hum. Brain Mapp. 41, 2014–2027. doi:10.1002/hbm.24926.
Günther, M., Oshio, K., Feinberg, D.A., 2005. Single-shot 3D imaging techniques improve arterial spin labeling perfusion measurements. Magn. Reson. Med. 54, 491–498. doi:10.1002/mrm.20580.
Hacker, C.D., Roland, J.L., Kim, A.H., Shimony, J.S., Leuthardt, E.C., 2019. Resting-state network mapping in neurosurgical practice: a review. Neurosurg. Focus 47, 1–9. doi:10.3171/2019.9.FOCUS19656.
Hale, J.R., Brookes, M.J., Hall, E.L., Zumer, J.M., Stevenson, C.M., Francis, S.T., Morris, P.G., 2010. Comparison of functional connectivity in default mode and sensorimotor networks at 3 and 7T. Magn. Reson. Mater. Phys., Biol. Med. 23, 339–349. doi:10.1007/s10334-010-0220-0.
Hargreaves, B.A., Cunningham, C.H., Nishimura, D.G., Conolly, S.M., 2004. Variable-rate selective excitation for rapid MRI sequences. Magn. Reson. Med. 52, 590–597. doi:10.1002/mrm.20168.
Harms, Michael P., Somerville, L.H., Ances, B.M., Andersson, J., Barch, D.M., Bastiani, M., Bookheimer, S.Y., Brown, T.B., Buckner, R.L., Burgess, G.C., Coalson, T.S., Chappell, M.A., Dapretto, M., Douaud, G., Fischl, B., Glasser, M.F., Greve, D.N., Hodge, C., Jamison, K.W., Jbabdi, S., Kandala, S., Li, X., Mair, R.W., Mangia, S., Marcus, D., Mascali, D., Moeller, S., Nichols, T.E., Robinson, E.C., Salat, D.H., Smith, S.M., Sotiropoulos, S.N., Terpstra, M., Thomas, K.M., Tisdall, M.D., Ugurbil, K., van der Kouwe, A., Woods, R.P., Zöllei, L., Van Essen, D.C., Yacoub, E., 2018. Extending the human connectome project across ages: imaging protocols for the lifespan development and aging projects. Neuroimage 183, 972–984. doi:10.1016/j.neuroimage.2018.09.060.
Heinzle, J., Kahnt, T., Haynes, J.D., 2011. Topographically specific functional connectivity between visual field maps in the human brain. Neuroimage 56, 1426–1436. doi:10.1016/j.neuroimage.2011.02.077.
Heinzle, J., Koopmans, P.J., den Ouden, H.E.M., Raman, S., Stephan, K.E., 2016. A hemodynamic model for layered BOLD signals. Neuroimage 125, 556–570. doi:10.1016/j.neuroimage.2015.10.025.
Hendriks, A.D., D'Agata, F., Raimondo, L., Schakel, T., Geerts, L., Luijten, P.R., Klomp, D.W.J., Petridou, N., 2020. Pushing functional MRI spatial and temporal resolution further: high-density receive arrays combined with shot-selective 2D CAIPIRINHA for 3D echo-planar imaging at 7 T. NMR Biomed. 33, 1–13. doi:10.1002/nbm.4281.
Hennig, J., Kiviniemi, V., Riemenschneider, B., Barghoorn, A., Akin, B., Wang, F., LeVan, P., 2020. 15 Years MR-encephalography. MAGMA doi:10.1007/s10334-020-00891-z.
Huang, P., Carlin, J.D., Alink, A., Kriegeskorte, N., Henson, R.N., Correia, M.M., 2018. Prospective motion correction improves the sensitivity of fMRI pattern decoding. Hum. Brain Mapp. 39, 4018–4031. doi:10.1002/hbm.24228.
Huber, L., Finn, E.S., Chai, Y., Goebel, R., Stirnberg, R., Stocker, T., Marrett, S., Uludag, K., Kim, S.G., Han, S., Bandettini, P.A., Poser, B.A., 2020. Layer-dependent functional connectivity methods. Prog. Neurobiol. 101835. doi:10.1016/j.pneurobio.2020.101835.
Huber, L., Goense, J., Kennerley, A.J., Trampel, R., Guidi, M., Reimer, E., Ivanov, D., Neef, N., Gauthier, C.J., Turner, R., Moller, H.E., 2015. Cortical lamina-dependent blood volume changes in human brain at 7 T. Neuroimage 107, 23–33. doi:10.1016/j.neuroimage.2014.11.046.
Huber, L., Handwerker, D.A., Jangraw, D.C., Chen, G., Hall, A., Stüber, C., Gonzalez-Castillo, J., Ivanov, D., Marrett, S., Guidi, M., Goense, J., Poser, B.A., Bandettini, P.A., 2017. High-resolution CBV-fMRI allows mapping of laminar activity and connectivity of cortical input and output in human M1. Neuron 96. doi:10.1016/j.neuron.2017.11.005, 1253-1263.e7.
Huber, L., Ivanov, D., Krieger, S.N., Streicher, M.N., Mildner, T., Poser, B.A., Möller, H.E., Turner, R., 2014. Slab-selective, BOLD-corrected VASO at 7 tesla provides measures of cerebral blood volume reactivity with high signal-to-noise ratio. Magn. Reson. Med. 72, 137–148. doi:10.1002/mrm.24916.
Huber, L., Tse, D.H.Y., Wiggins, C.J., Uludağ, K., Kashyap, S., Jangraw, D.C., Bandettini, P.A., Poser, B.A., Ivanov, D., 2018. Ultra-high resolution blood volume fMRI and BOLD fMRI in humans at 9.4 T: capabilities and challenges. Neuroimage 178, 769–779. doi:10.1016/j.neuroimage.2018.06.025.
Huotari, N., Raitamaa, L., Helakari, H., Kananen, J., Raatikainen, V., Rasila, A., Tuovinen, T., Kantola, J., Borchardt, V., Kiviniemi, V.J., Korhonen, V.O., 2019. Sampling Rate Effects on Resting State fMRI Metrics. Front. Neurosci. 13, 279. doi:10.3389/fnins.2019.00279.
Ivanov, D., Gardumi, A., Haast, R.A.M., Pfeuffer, J., Poser, B.A., Uludag, K., 2017. Comparison of 3T and 7T ASL techniques for concurrent functional perfusion and BOLD studies. Neuroimage 156, 363–376. doi:10.1016/j.neuroimage.2017.05.038.
Jacobs, H.I., Priovoulos, N., Poser, B.A., Pagen, L.H., Ivanov, D., Verhey, F.R., Uludag, K., 2020. Dynamic behavior of the locus coeruleus during arousal-related memory processing in a multi-modal 7T fMRI paradigm. Elife 9. doi:10.7554/eLife.52059.
Jacobs, J., Stich, J., Zahneisen, B., Asslander, J., Ramantani, G., Schulze-Bonhage, A., Korinthenberg, R., Hennig, J., LeVan, P., 2014. Fast fMRI provides high statistical power in the analysis of epileptic networks. Neuroimage 88, 282–294. doi:10.1016/j.neuroimage.2013.10.018.
Jahanian, H., Holdsworth, S., Christen, T., Wu, H., Zhu, K., Kerr, A.B., Middione, M.J., Dougherty, R.F., Moseley, M., Zaharchuk, G., 2019. Advantages of short repetition time resting-state functional MRI enabled by simultaneous multi-slice imaging. J. Neurosci. Methods 311, 122–132. doi:10.1016/j.jneumeth.2018.09.033.
Jann, K., Gee, D.G., Kilroy, E., Schwab, S., Smith, R.X., Cannon, T.D., Wang, D.J.J.J., 2015. Functional connectivity in BOLD and CBF data: Similarity and reliability of resting brain networks. Neuroimage 106, 111–122. doi:10.1016/j.neuroimage.2014.11.028.
Jann, K., Smith, R.X., Rios Piedra, E.A., Dapretto, M., Wang, D.J.J., 2016. Noise reduction in arterial spin labeling based functional connectivity using nuisance variables. Front. Neurosci. 10. doi:10.3389/fnins.2016.00371.
Jao, T., Vértes, P.E., Alexander-Bloch, A.F., Tang, I.-N., Yu, Y.-C., Chen, J.-H., Bullmore, E.T., 2013. Volitional eyes opening perturbs brain dynamics and functional connectivity regardless of light input. Neuroimage 69, 21–34. doi:10.1016/j.neuroimage.2012.12.007.
Jensen, J.H., Lu, H., Inglese, M., 2006. Microvessel density estimation in the human brain by means of dynamic contrast-enhanced echo-planar imaging. Magn. Reson. Med. 56, 1145–1150. doi:10.1002/mrm.21052.
Jiang, Y., Song, L., Li, X., Zhang, Y., Chen, Y., Jiang, S., Hou, C., Yao, D., Wang, X., Luo, C., 2019. Dysfunctional white-matter networks in medicated and unmedicated benign epilepsy with centrotemporal spikes. Hum. Brain Mapp. 40, 3113–3124. doi:10.1002/hbm.24584.
Jin, T., Kim, S.-G., 2008. Cortical layer-dependent dynamic blood oxygenation, cerebral blood flow and cerebral blood volume responses during visual stimulation. Neuroimage 43, 1–9. doi:10.1016/j.neuroimage.2008.06.029.
Jones, D.T., Vemuri, P., Murphy, M.C., Gunter, J.L., Senjem, M.L., Machulda, M.M., Przybelski, S.A., Gregg, B.E., Kantarci, K., Knopman, D.S., Boeve, B.F., Petersen, R.C., Jack Jr., C.R., 2012. Non-stationarity in the "resting brain's" modular architecture. PLoS One 7, e39731. doi:10.1371/journal.pone.0039731.
Jorge, J., Figueiredo, P., van der Zwaag, W., Marques, J.P., 2013. Signal fluctuations in fMRI data acquired with 2D-EPI and 3D-EPI at 7 Tesla. Magn. Reson. Imaging 31, 212–220. doi:10.1016/j.mri.2012.07.001.
Kashyap, S., Ivanov, D., Havlicek, M., Poser, B.A., Uludag, K., 2018. Impact of acquisition

and analysis strategies on cortical depth-dependent fMRI. Neuroimage 168, 332–344. doi:10.1016/j.neuroimage.2017.05.022.
Kay, K., Jamison, K.W., Vizioli, L., Zhang, R., Margalit, E., Ugurbil, K., 2019. A critical assessment of data quality and venous effects in sub-millimeter fMRI. Neuroimage 189, 847–869. doi:10.1016/j.neuroimage.2019.02.006.
Kay, K., Jamison, K.W., Zhang, R.Y., Ugurbil, K., 2020. A temporal decomposition method for identifying venous effects in task-based fMRI. Nat. Methods 17, 1033–1039. doi:10.1038/s41592-020-0941-6.
Khatamian, Y.B., Golestani, A.M., Ragot, D.M., Chen, J.J., 2016. Spin-echo resting-state functional connectivity in high-susceptibility regions: accuracy, reliability, and the impact of physiological noise. Brain Connect. 6, 283–297. doi:10.1089/brain.2015.0365.
Kindler, J., Jann, K., Homan, P., Hauf, M., Walther, S., Strik, W., Dierks, T., Hubl, D., 2015. Static and dynamic characteristics of cerebral blood flow during the resting state in schizophrenia. Schizophr. Bull. 41, 163–170. doi:10.1093/schbul/sbt180.
Kirilina, E., Lutti, A., Poser, B.A., Blankenburg, F., Weiskopf, N., 2016. The quest for the best: the impact of different EPI sequences on the sensitivity of random effect fMRI group analyses. Neuroimage 126, 49–59. doi:10.1016/j.neuroimage.2015.10.071.
Knapen, T., 2021. Topographic connectivity reveals task-dependent retinotopic processing throughout the human brain. Proc. Natl. Acad. Sci. USA 118, 1–6. doi:10.1073/pnas.2017032118.
Koopmans, P.J., Boyacioğlu, R., Barth, M., Norris, D.G., 2012. Whole brain, high resolution spin-echo resting state fMRI using PINS multiplexing at 7T. Neuroimage 62, 1939–1946. doi:10.1016/j.neuroimage.2012.05.080.
Kumar, A., Edelstein, W.A., Bottomley, P.A., 2009. Noise figure limits for circular loop MR coils. Magn. Reson. Med. 61, 1201–1209. doi:10.1002/mrm.21948.
Kundu, P., Benson, B.E., Rosen, D., Frangou, S., Leibenluft, E., Luh, W.M., Bandettini, P.A., Pine, D.S., Ernst, M., 2018. The integration of functional brain activity from adolescence to adulthood. J. Neurosci. 38, 3559–3570. doi:10.1523/JNEUROSCI.1864-17.2018.
Kundu, P., Inati, S.J., Evans, J.W., Luh, W.M., Bandettini, P.A., 2012. Differentiating BOLD and non-BOLD signals in fMRI time series using multi-echo EPI. Neuroimage 60, 1759–1770. doi:10.1016/j.neuroimage.2011.12.028.
Kundu, P., Voon, V., Balchandani, P., Lombardo, M.V., Poser, B.A., Bandettini, P.A., 2017. Multi-echo fMRI: a review of applications in fMRI denoising and analysis of BOLD signals. Neuroimage 154, 59–80. doi:10.1016/j.neuroimage.2017.03.033.
Lanka, P., Deshpande, G., 2019. Combining Prospective Acquisition CorrEction (PACE) with retrospective correction to reduce motion artifacts in resting state fMRI data. Brain Behav. 9, 1–21. doi:10.1002/brb3.1341.
Larkum, M.E., Petro, L.S., Sachdev, R.N.S., Muckli, L., 2018. A perspective on cortical layering and layer-spanning neuronal elements. Front. Neuroanat. 12. doi:10.3389/fnana.2018.00056.
Lee, H.L., Zahneisen, B., Hugger, T., LeVan, P., Hennig, J., 2013. Tracking dynamic resting-state networks at higher frequencies using MR-encephalography. Neuroimage 65, 216–222. doi:10.1016/j.neuroimage.2012.10.015.
Lee, J., Gebhardt, M., Wald, L.L., Adalsteinsson, E., 2012. Local SAR in parallel transmission pulse design. Magn. Reson. Med. 67, 1566–1578. doi:10.1002/mrm.23140.
Lee, M.H., Smyser, C.D., Shimony, J.S., 2013. Resting-state fMRI: a review of methods and clinical applications. Am. J. Neuroradiol. 34, 1866–1872. doi:10.3174/ajnr.A3263.
Li, M., Gao, Y., Gao, F., Anderson, A.W., Ding, Z., Gore, J.C., 2020. Functional engagement of white matter in resting-state brain networks. Neuroimage 220, 117096. doi:10.1016/j.neuroimage.2020.117096.
Liang, X., Connelly, A., Calamante, F., 2015. Voxel-wise functional connectomics using arterial spin labeling functional magnetic resonance imaging: the role of denoising. Brain Connect. 5, 543–553. doi:10.1089/brain.2014.0290.
Liang, X., Connelly, A., Calamante, F., 2014. Graph analysis of resting-state ASL perfusion MRI data: nonlinear correlations among CBF and network metrics. Neuroimage 87, 265–275. doi:10.1016/j.neuroimage.2013.11.013.
Liang, X., Tournier, J.D., Masterton, R., Connelly, A., Calamante, F., 2012. A k-space sharing 3D GRASE pseudocontinuous ASL method for whole-brain resting-state functional connectivity. Int. J. Imaging Syst. Technol. 22, 37–43. doi:10.1002/ima.22006.
Lin, F.H., Tsai, K.W.K., Chu, Y.H., Witzel, T., Nummenmaa, A., Raij, T., Ahveninen, J., Kuo, W.J., Belliveau, J.W., 2012. Ultrafast inverse imaging techniques for fMRI. Neuroimage 62, 699–705. doi:10.1016/j.neuroimage.2012.01.072.
Lin, H., Li, M., Zhan, Y., Lin, L., Yang, K., Hu, S., Han, Y., 2020. Disrupted white matter functional connectivity in aMCI APOEε4 carriers: a resting-state study. Brain Imaging Behav. doi:10.1007/s11682-020-00367-7.
Lombardo, M.V., Auyeung, B., Holt, R.J., Waldman, J., Ruigrok, A.N.V., Mooney, N., Bullmore, E.T., Baron-Cohen, S., Kundu, P., 2016. Improving effect size estimation and statistical power with multi-echo fMRI and its impact on understanding the neural systems supporting mentalizing. Neuroimage 142, 55–66. doi:10.1016/j.neuroimage.2016.07.022.
Lu, H., Golay, X., Pekar, J.J., van Zijl, P.C.M.M., Van Zijl, P.C.M., van Zijl, P.C.M.M., 2003. Functional magnetic resonance imaging based on changes in vascular space occupancy. Magn. Reson. Med. 50, 263–274. doi:10.1002/mrm.10519.
Lynch, C.J., Power, J.D., Scult, M.A., Dubin, M., Gunning, F.M., Liston, C., 2020. Rapid precision functional mapping of individuals using multi-echo fMRI. Cell Rep. 33, 108540. doi:10.1016/j.celrep.2020.108540.
Markuerkiaga, I., Barth, M., Norris, D.G., 2016. A cortical vascular model for examining the specificity of the laminar BOLD signal. Neuroimage 132, 491–498. doi:10.1016/j.neuroimage.2016.02.073.
Marquardt, I., Schneider, M., Gulban, O.F., Ivanov, D., Uludag, K., 2018. Cortical depth profiles of luminance contrast responses in human V1 and V2 using 7 T fMRI. Hum. Brain Mapp. 39, 2812–2827. doi:10.1002/hbm.24042.
Marussich, L., Lu, K.H., Wen, H., Liu, Z., 2017. Mapping white-matter functional organization at rest and during naturalistic visual perception. Neuroimage 146, 1128–1141. doi:10.1016/j.neuroimage.2016.10.005.
Maziero, D., Rondinoni, C., Marins, T., Stenger, V.A., Ernst, T., 2020. Prospective motion correction of fMRI: Improving the quality of resting state data affected by large head motion. Neuroimage 212, 116594. doi:10.1016/j.neuroimage.2020.116594.
McNab, J.A., Edlow, B.L., Witzel, T., Huang, S.Y., Bhat, H., Heberlein, K., Feiweier, T., Liu, K., Keil, B., Cohen-Adad, J., Tisdall, M.D., Folkerth, R.D., Kinney, H.C., Wald, L.L., 2013. The human connectome project and beyond: initial applications of 300 mT/m gradients. Neuroimage 80, 234–245. doi:10.1016/j.neuroimage.2013.05.074.
Miao, X., Gu, H., Yan, L., Lu, H., Wang, D.J.J.J., Zhou, X.J., Zhuo, Y., Yang, Y., 2014. Detecting resting-state brain activity by spontaneous cerebral blood volume fluctuations using whole brain vascular space occupancy imaging. Neuroimage 84, 575–584. doi:10.1016/j.neuroimage.2013.09.019.
Moeller, S., Yacoub, E., Olman, C.A., Auerbach, E., Strupp, J., Harel, N., Ugurbil, K., 2010. Multiband multislice GE-EPI at 7 tesla, with 16-fold acceleration using partial parallel imaging with application to high spatial and temporal whole-brain fMRI. Magn. Reson. Med. 63, 1144–1153. doi:10.1002/mrm.22361.
Morris, L.S., Costi, S., Tan, A., Stern, E.R., Charney, D.S., Murrough, J.W., 2020. Ketamine normalizes subgenual cingulate cortex hyper-activity in depression. Neuropsychopharmacology 45, 975–981. doi:10.1038/s41386-019-0591-5.
Morris, L.S., Kundu, P., Baek, K., Irvine, M.A., Mechelmans, D.J., Wood, J., Harrison, N.A., Robbins, T.W., Bullmore, E.T., Voon, V., 2016. Jumping the gun: mapping neural correlates of waiting impulsivity and relevance across alcohol misuse. Biol. Psychiatry 79, 499–507. doi:10.1016/j.biopsych.2015.06.009.
Morris, L.S., Kundu, P., Costi, S., Collins, A., Schneider, M., Verma, G., Balchandani, P., Murrough, J.W., 2019. Ultra-high field MRI reveals mood-related circuit disturbances in depression: a comparison between 3-Tesla and 7-Tesla. Transl. Psychiatry 9. doi:10.1038/s41398-019-0425-6.
Napadow, V., Dhond, R., Conti, G., Makris, N., Brown, E.N., Barbieri, R., 2008. Brain correlates of autonomic modulation: combining heart rate variability with fMRI. Neuroimage 42, 169–177. doi:10.1016/j.neuroimage.2008.04.238.
Narsude, M., Gallichan, D., van der Zwaag, W., Gruetter, R., Marques, J.P., 2016. Three-dimensional echo planar imaging with controlled aliasing: a sequence for high temporal resolution functional MRI. Magn. Reson. Med. 75, 2350–2361. doi:10.1002/mrm.25835.
Narsude, M., van der Zwaag, W., Gallichan, D., Gruetter, R., Marques, J., 2014. Resting state networks detection, the importance of high temporal resolution: a comparison study between 2D-EPI, SMS 2D-EPI and 3D-EPI-CAIPI acquisitions. Proc. Intl. Soc. Mag. Reson. Med. 4325.
Newton, A.T., Rogers, B.P., Gore, J.C., Morgan, V.L., 2012. Improving measurement of functional connectivity through decreasing partial volume effects at 7T. Neuroimage 59, 2511–2517. doi:10.1016/j.neuroimage.2011.08.096.
Nir, T., Jacob, Y., Huang, K.-H., Schwartz, A.E., Brallier, J.W., Ahn, H., Kundu, P., Tang, C.Y., Delman, B.N., McCormick, P.J., Sano, M., Deiner, S., Baxter, M.G., Mincer, J.S., 2020. Resting-state functional connectivity in early postanaesthesia recovery is characterised by globally reduced anticorrelations. Br. J. Anaesth. 125, 529–538. doi:10.1016/j.bja.2020.06.058.
Norris, D.G., 2012. Spin-echo fMRI: the poor relation? Neuroimage 62, 1109–1115. doi:10.1016/j.neuroimage.2012.01.003.
Norris, D.G., Koopmans, P.J., Boyacioğlu, R., Barth, M., 2011. Power Independent of Number of Slices (PINS) radiofrequency pulses for low-power simultaneous multislice excitation. Magn. Reson. Med. 66, 1234–1240. doi:10.1002/mrm.23152.
Ogawa, S., Menon, R.S., Tank, D.W., Kim, S.G., Merkle, H., Ellermann, J.M., Ugurbil, K., 1993. Functional brain mapping by blood oxygenation level-dependent contrast magnetic resonance imaging. A comparison of signal characteristics with a biophysical model. Biophys. J. 64, 803–812. doi:10.1016/S0006-3495(93)81441-3.
Oliveira, Í.A.F., Guimarães, T.M., Souza, R.M., dos Santos, A.C., Machado-de-Sousa, J.P., Hallak, J.E.C., Leoni, R.F., 2018. Brain functional and perfusional alterations in schizophrenia: an arterial spin labeling study. Psychiatry Res. Neuroimaging 272, 71–78. doi:10.1016/j.pscychresns.2017.12.001.
Oliveira, Í.A.F., van der Zwaag, W., Raimondo, L., Dumoulin, S.O., Siero, J.C.W., 2021. Comparing hand movement rate dependence of cerebral blood volume and BOLD responses at 7T. Neuroimage 226, 117623. doi:10.1016/j.neuroimage.2020.117623.
Overton, D.J., Bhagwat, N., Viviano, J.D., Jacobs, G.R., Voineskos, A.N., 2020. Identifying psychosis spectrum youth using support vector machines and cerebral blood perfusion as measured by arterial spin labeled fMRI. NeuroImage Clin. 27, 102304. doi:10.1016/j.nicl.2020.102304.
Pais-Roldán, P., Yun, S.D., Palomero-Gallagher, N., Shah, N.J., 2020. Cortical depth-dependent human fMRI of resting-state networks using EPIK. bioRxiv doi:10.1101/2020.12.07.414144, 2020.12.07.414144.
Pannunzi, M., Hindriks, R., Bettinardi, R.G., Wenger, E., Lisofsky, N., Martensson, J., Butler, O., Filevich, E., Becker, M., Lochstet, M., Kühn, S., Deco, G., 2017. Resting-state fMRI correlations:from link-wise unreliability to whole brain stability. Neuroimage 157, 250–262. doi:10.1016/j.neuroimage.2017.06.006.
Patriat, R., Molloy, E.K., Meier, T.B., Kirk, G.R., Nair, V.A., Meyerand, M.E., Prabhakaran, V., Birn, R.M., 2013. The effect of resting condition on resting-state fMRI reliability and consistency: a comparison between resting with eyes open, closed, and fixated. Neuroimage 78, 463–473. doi:10.1016/j.neuroimage.2013.04.013.
Peltier, S.J., Noll, D.C., 2002. T2* dependence of low frequency functional connectivity. Neuroimage 16, 985–992 https://doi.org/10.1006/nimg.2002.1141.
Petridou, N., Italiaander, M., van de Bank, B.L., Siero, J.C.W., Luijten, P.R., Klomp, D.W.J., 2013. Pushing the limits of high-resolution functional MRI using a simple high-density multi-element coil design. NMR Biomed. 26, 65–73. doi:10.1002/nbm.2820.
Petridou, N., Siero, J.C.W., 2019. Laminar fMRI: what can the time domain tell us? Neuroimage 197, 761–771. doi:10.1016/j.neuroimage.2017.07.040.

Pinto, J., Nunes, S., Bianciardi, M., Dias, A., Silveira, L.M., Wald, L.L., Figueiredo, P., 2017. Improved 7 Tesla resting-state fMRI connectivity measurements by cluster-based modeling of respiratory volume and heart rate effects. Neuroimage 153, 262–272 https://doi.org/10.1016/j.neuroimage.2017.04.009.
Pohmann, R., Speck, O., Scheffler, K., 2016. Signal-to-noise ratio and MR tissue parameters in human brain imaging at 3, 7, and 9.4 tesla using current receive coil arrays. Magn. Reson. Med. 75, 801–809. doi:10.1002/mrm.25677.
Polimeni, J.R., Fischl, B., Greve, D.N., Wald, L.L., 2010. Laminar analysis of 7T BOLD using an imposed spatial activation pattern in human V1. Neuroimage 52, 1334–1346. doi:10.1016/j.neuroimage.2010.05.005.
Poser, B.A., Anderson, R.J., Guérin, B., Setsompop, K., Deng, W., Mareyam, A., Serano, P., Wald, L.L., Stenger, V.A., 2014. Simultaneous multislice excitation by parallel transmission. Magn. Reson. Med. 71, 1416–1427. doi:10.1002/mrm.24791.
Poser, B.A., Koopmans, P.J., Witzel, T., Wald, L.L., Barth, M., 2010. Three dimensional echo-planar imaging at 7 Tesla. Neuroimage 51, 261–266. doi:10.1016/j.neuroimage.2010.01.108.
Poser, B.A., Norris, D.G., 2009. 3D single-shot VASO using a maxwell gradient compensated GRASE sequence. Magn. Reson. Med. 62, 255–262. doi:10.1002/mrm.22000.
Poser, B.A., Norris, D.G., 2007. Fast spin echo sequences for BOLD functional MRI. Magn. Reson. Mater. Physics, Biol. Med. 20, 11–17. doi:10.1007/s10334-006-0063-x.
Poser, B.A., Versluis, M.J., Hoogduin, J.M., Norris, D.G., 2006. BOLD contrast sensitivity enhancement and artifact reduction with multiecho EPI: Parallel-acquired inhomogeneity-desensitized fMRI. Magn. Reson. Med. 55, 1227–1235. doi:10.1002/mrm.20900.
Posse, S., 2012. Multi-echo acquisition. Neuroimage 62, 665–671 https://doi.org/10.1016/j.neuroimage.2011.10.057.
Power, J.D., Plitt, M., Gotts, S.J., Kundu, P., Voon, V., Bandettini, P.A., Martin, A., 2018. Ridding fMRI data of motion-related influences: removal of signals with distinct spatial and physical bases in multiecho data. Proc. Natl. Acad. Sci. USA 115, E2105–E2114. doi:10.1073/pnas.1720985115.
Power, J.D., Silver, B.M., Silverman, M.R., Ajodan, E.L., Bos, D.J., Jones, R.M., 2019. Customized head molds reduce motion during resting state fMRI scans. Neuroimage 189, 141–149. doi:10.1016/j.neuroimage.2019.01.016.
Preibisch, C., Castrillon, G.J., Buhrer, M., Riedl, V., 2015. Evaluation of multiband EPI acquisitions for resting state fMRI. PLoS One 10, e0136961. doi:10.1371/journal.pone.0136961.
Preti, M.G., Bolton, T.A., Ville, D.V, 2016. The dynamic functional connectome: state-of-the-art and perspectives. Neuroimage doi:10.1016/j.neuroimage.2016.12.061.
Priovoulos, N., Roos, T., Ipek, Ö., Meliado, E.F., Nkrumah, R.O., Klomp, D.W.J., van der Zwaag, W., 2021. A local multi-transmit coil combined with a high-density receive array for cerebellar fMRI at 7 T. NMR Biomed. 1–13. doi:10.1002/nbm.4586.
Raemaekers, M., Schellekens, W., van Wezel, R.J.A., Petridou, N., Kristo, G., Ramsey, N.F., 2014. Patterns of resting state connectivity in human primary visual cortical areas: A 7T fMRI study. Neuroimage 84, 911–921. doi:10.1016/j.neuroimage.2013.09.060.
Reynaud, O., Jorge, J., Gruetter, R., Marques, J.P., van der Zwaag, W., 2017. Influence of physiological noise on accelerated 2D and 3D resting state functional MRI data at 7 T. Magn. Reson. Med. 78, 888–896. doi:10.1002/mrm.26823.
Roemer, P.B., Edelstein, W.A., Hayes, C.E., Souza, S.P., Mueller, O.M., 1990. The NMR phased array. Magn. Reson. Med. 16, 192–225. doi:10.1002/mrm.1910160203.
Salomon, R., Darulova, J., Narsude, M., van der Zwaag, W., 2014. Comparison of an 8-channel and a 32-channel coil for high-resolution FMRI at 7 T. Brain Topogr. 27, 209–212. doi:10.1007/s10548-013-0298-6.
Setsompop, K., Feinberg, D.A., Polimeni, J.R., 2016. Rapid brain MRI acquisition techniques at ultra-high fields. NMR Biomed. 29, 1198–1221. doi:10.1002/nbm.3478.
Setsompop, K., Gagoski, B.A., Polimeni, J.R., Witzel, T., Wedeen, V.J., Wald, L.L., 2012. Blipped-controlled aliasing in parallel imaging for simultaneous multislice echo planar imaging with reduced g-factor penalty. Magn. Reson. Med. 67, 1210–1224. doi:10.1002/mrm.23097.
Shamir, I., Assaf, Y., 2020. An MRI-based, data-driven model of cortical laminar connectivity. Neuroinformatics doi:10.1007/s12021-020-09491-7.
Sharoh, D., van Mourik, T., Bains, L.J., Segaert, K., Weber, K., Hagoort, P., Norris, D.G., 2019. Laminar specific fMRI reveals directed interactions in distributed networks during language processing. Proc. Natl. Acad. Sci. 116, 21185–21190. doi:10.1073/pnas.1907858116.
Silva, J.P.S., Mônaco, L.da M., Paschoal, A.M., Oliveira, Í.A.F.de, Leoni, R.F., 2018. Effects of global signal regression and subtraction methods on resting-state functional connectivity using arterial spin labeling data. Magn. Reson. Imaging 51, 151–157. doi:10.1016/j.mri.2018.05.006.
Smith, S.M., Beckmann, C.F., Andersson, J., Auerbach, E.J., Bijsterbosch, J., Douaud, G., Duff, E., Feinberg, D.A., Griffanti, L., Harms, M.P., Kelly, M., Laumann, T., Miller, K.L., Moeller, S., Petersen, S., Power, J., Salimi-Khorshidi, G., Snyder, A.Z., Vu, A.T., Woolrich, M.W., Xu, J., Yacoub, E., Uğurbil, K., Van Essen, D.C., Glasser, M.F., 2013. Resting-state fMRI in the human connectome project. Neuroimage 80, 144–168. doi:10.1016/j.neuroimage.2013.05.039.
Smith, Stephen M, Vidaurre, D., Beckmann, C.F., Glasser, M.F., Jenkinson, M., Miller, K.L., Nichols, T.E., Robinson, E.C., Salimi-Khorshidi, G., Woolrich, M.W., Barch, D.M., Uğurbil, K., Van Essen, D.C., 2013. Functional connectomics from resting-state fMRI. Trends Cogn. Sci. 17, 666–682. doi:10.1016/j.tics.2013.09.016.
Smitha, K.A., Arun, K.M., Rajesh, P.G., Joel, S.E., Venkatesan, R., Thomas, B., Kesavadas, C., 2018. Multiband fMRI as a plausible, time-saving technique for resting-state data acquisition: Study on functional connectivity mapping using graph theoretical measures. Magn. Reson. Imaging 53, 1–6. doi:10.1016/j.mri.2018.06.013.
Stirnberg, R., Brenner, D., Stöcker, T., Shah, N.J., 2016. Rapid fat suppression for three-dimensional echo planar imaging with minimized specific absorption rate. Magn. Reson. Med. 76, 1517–1523. doi:10.1002/mrm.26063.
Stirnberg, R., Huijbers, W., Brenner, D., Poser, B.A., Breteler, M., Stocker, T., 2017. Rapid whole-brain resting-state fMRI at 3 T: Efficiency-optimized three-dimensional EPI versus repetition time-matched simultaneous-multi-slice EPI. Neuroimage 163, 81–92. doi:10.1016/j.neuroimage.2017.08.031.
Tan, E.T., Lee, S.K., Weavers, P.T., Graziani, D., Piel, J.E., Shu, Y., Huston 3rd, J., Bernstein, M.A., Foo, T.K., 2016. High slew-rate head-only gradient for improving distortion in echo planar imaging: preliminary experience. J. Magn. Reson. Imaging 44, 653–664. doi:10.1002/jmri.25210.
Todd, N., Moeller, S., Auerbach, E.J., Yacoub, E., Flandin, G., Weiskopf, N., 2016. Evaluation of 2D multiband EPI imaging for high-resolution, whole-brain, task-based fMRI studies at 3T: sensitivity and slice leakage artifacts. Neuroimage 124, 32–42. doi:10.1016/j.neuroimage.2015.08.056.
Togo, H., Rokicki, J., Yoshinaga, K., Hisatsune, T., Matsuda, H., Haga, N., Hanakawa, T., 2017. Effects of field-map distortion correction on resting state functional connectivity MRI. Front. Neurosci. 11, 1–10. doi:10.3389/fnins.2017.00656.
Torrisi, S., Nord, C.L., Balderston, N.L., Roiser, J.P., Grillon, C., Ernst, M., 2017. Resting state connectivity of the human habenula at ultra-high field. Neuroimage 147, 872–879. doi:10.1016/j.neuroimage.2016.10.034.
Triantafyllou, C., Polimeni, J.R., Wald, L.L., 2011. Physiological noise and signal-to-noise ratio in fMRI with multi-channel array coils. Neuroimage 55, 597–606. doi:10.1016/j.neuroimage.2010.11.084.
Turner, R., 2002. How much cortex can a vein drain? Downstream dilution of activation-related cerebral blood oxygenation changes. Neuroimage 16, 1062–1067. doi:10.1006/nimg.2002.1082.
Uludağ, K., Blinder, P., 2018. Linking brain vascular physiology to hemodynamic response in ultra-high field MRI. Neuroimage 168, 279–295. doi:10.1016/j.neuroimage.2017.02.063.
Vaidya, M.V, Collins, C.M., Sodickson, D.K., Brown, R., Wiggins, G.C., Lattanzi, R., 2016. Dependence of B1+ and B1- field patterns of surface coils on the electrical properties of the sample and the MR operating frequency. Concepts Magn. Reson. Part B Magn. Reson. Eng. 46, 25–40. doi:10.1002/cmr.b.21319.
Van de Moortele, P.F., Auerbach, E.J., Olman, C., Yacoub, E., Uğurbil, K., Moeller, S., 2009. T1 weighted brain images at 7 Tesla unbiased for Proton Density, T2* contrast and RF coil receive B1 sensitivity with simultaneous vessel visualization. Neuroimage 46, 432–446. doi:10.1016/j.neuroimage.2009.02.009.
van den Heuvel, M.P., Hulshoff Pol, H.E., 2010. Exploring the brain network: a review on resting-state fMRI functional connectivity. Eur. Neuropsychopharmacol. 20, 519–534. doi:10.1016/j.euroneuro.2010.03.008.
van der Zwaag, W., Marques, J.P., Hergt, M., Gruetter, R., 2009. Investigation of high-resolution functional magnetic resonance imaging by means of surface and array radiofrequency coils at 7 T. Magn. Reson. Imaging 27, 1011–1018. doi:10.1016/j.mri.2009.01.013.
van der Zwaag, W., Marques, J.P., Kober, T., Glover, G., Gruetter, R., Krueger, G., 2012. Temporal SNR characteristics in segmented 3D-EPI at 7T. Magn. Reson. Med. 67, 344–352. doi:10.1002/mrm.23007.
van der Zwaag, W., Reynaud, O., Narsude, M., Gallichan, D., Marques, J.P., 2018. High spatio-temporal resolution in functional MRI with 3D echo planar imaging using cylindrical excitation and a CAIPIRINHA undersampling pattern. Magn. Reson. Med. 79, 2589–2596. doi:10.1002/mrm.26906.
van Dijk, J A, Fracasso, A., Petridou, N., Dumoulin, S.O., 2020. Linear systems analysis for laminar fMRI: evaluating BOLD amplitude scaling for luminance contrast manipulations. Sci. Rep. 10, 5462. doi:10.1038/s41598-020-62165-x.
Van Dijk, K.R., Sabuncu, M.R., Buckner, R.L., 2012. The influence of head motion on intrinsic functional connectivity MRI. Neuroimage 59, 431–438. doi:10.1016/j.neuroimage.2011.07.044.
Van Dijk, K.R.A., Hedden, T., Venkataraman, A., Evans, K.C., Lazar, S.W., Buckner, R.L., 2010. Intrinsic functional connectivity as a tool for human connectomics: theory, properties, and optimization. J. Neurophysiol. 103, 297–321. doi:10.1152/jn.00783.2009.
Van Osch, M.J.P., Teeuwisse, W.M., Van Walderveen, M.A.A., Hendrikse, J., Kies, D.A., Van Buchem, M.A., 2009. Can arterial spin labeling detect white matter perfusion signal? Magn. Reson. Med. 62, 165–173. doi:10.1002/mrm.22002.
Váša, F., Romero-Garcia, R., Kitzbichler, M.G., Seidlitz, J., Whitaker, K.J., Vaghi, M.M., Kundu, P., Patel, A.X., Fonagy, P., Dolan, R.J., Jones, P.B., Goodyer, I.M., Vértes, P.E., Bullmore, E.T., 2020. Conservative and disruptive modes of adolescent change in human brain functional connectivity. Proc. Natl. Acad. Sci. USA 117, 3248–3253. doi:10.1073/pnas.1906144117.
Vaughan, J.T., Garwood, M., Collins, C.M., Liu, W., Delabarre, L., Adriany, G., Andersen, P., Merkle, H., Goebel, R., Smith, M.B., Ugurbil, K., 2001. 7T vs. 4T: RF power, homogeneity, and signal-to-noise comparison in head images. Magn. Reson. Med. 46, 24–30. doi:10.1002/mrm.1156.
Vidorreta, M., Wang, Z., Rodriguez, I., Pastor, M.A., Detre, J.A., Fernández-Seara, M.A., 2013. Comparison of 2D and 3D single-shot ASL perfusion fMRI sequences. Neuroimage 66, 662–671. doi:10.1016/j.neuroimage.2012.10.087.
Viviani, R., Messina, I., Walter, M., 2011. Resting state functional connectivity in perfusion imaging: correlation maps with Bold connectivity and resting state perfusion. PLoS One 6. doi:10.1371/journal.pone.0027050.
Wald, L.L., 2012. The future of acquisition speed, coverage, sensitivity, and resolution. Neuroimage 62, 1221–1229. doi:10.1016/j.neuroimage.2012.02.077.
Wallace, T.E., Polimeni, J.R., Stockmann, J.P., Hoge, W.S., Kober, T., Warfield, S.K., Afacan, O., 2021. Dynamic distortion correction for functional MRI using FID navigators. Magn. Reson. Med. 85, 1294–1307. doi:10.1002/mrm.28505.
Wang, T., Wilkes, D.M., Li, M., Wu, X., Gore, J.C., Ding, Z., 2020. Hemodynamic response function in brain white matter in a resting state. Cereb. Cortex Commun. 1, 1–13. doi:10.1093/texcom/tgaa056.
Wang, Z., Aguirre, G.K., Rao, H., Wang, J., Fernández-Seara, M.A., Childress, A.R., Detre, J.A., 2008. Empirical optimization of ASL data analysis using an

ASL data processing toolbox: ASLtbx. Magn. Reson. Imaging 26, 261–269. doi:10.1016/j.mri.2007.07.003.

Weng, Y., Liu, X., Hu, H., Huang, H., Zheng, S., Chen, Q., Song, J., Cao, B., Wang, J., Wang, S., Huang, R., 2020. Open eyes and closed eyes elicit different temporal properties of brain functional networks. Neuroimage 222, 117230. doi:10.1016/j.neuroimage.2020.117230.

Wiggins, G.C., Polimeni, J.R., Potthast, A., Schmitt, M., Alagappan, V., Wald, L.L., 2009. 96-Channel receive-only head coil for 3 Tesla: design optimization and evaluation. Magn. Reson. Med. 62, 754–762. doi:10.1002/mrm.22028.

Wong, E.C., 2012. Local head gradient coils: window(s) of opportunity. Neuroimage 62, 660–664. doi:10.1016/j.neuroimage.2012.01.025.

Wu, G.R., Marinazzo, D., 2016. Sensitivity of the resting-state haemodynamic response function estimation to autonomic nervous system fluctuations. Philos. Trans. A Math. Phys. Eng. Sci. 374. doi:10.1098/rsta.2015.0190.

Wu, P.-Y., Chu, Y.-H., Lin, J.-F.L., Kuo, W.-J., Lin, F.-H., 2018. Feature-dependent intrinsic functional connectivity across cortical depths in the human auditory cortex. Sci. Rep. 8, 13287. doi:10.1038/s41598-018-31292-x.

Wu, X., Auerbach, E.J., Vu, A.T., Moeller, S., Van de Moortele, P.F., Yacoub, E., Uğurbil, K., 2019. Human connectome project-style resting-state functional MRI at 7 Tesla using radiofrequency parallel transmission. Neuroimage 184, 396–408. doi:10.1016/j.neuroimage.2018.09.038.

Wu, X., Tian, J., Schmitter, S., Vaughan, J.T., Uğurbil, K., Van de Moortele, P.F., 2016. Distributing coil elements in three dimensions enhances parallel transmission multiband RF performance: a simulation study in the human brain at 7 Tesla. Magn. Reson. Med. 75, 2464–2472. doi:10.1002/mrm.26194.

Xu, H., Li, J., Chen, K., Zhu, H., Luo, L., Yang, L., Chen, F., Ma, H., Qu, X., Li, Z., Zhang, R., 2021. Changes in resting-state cerebral blood flow and its connectivity in patients with focal to bilateral tonic-clonic seizures. Epilepsy Behav. 115, 107687. doi:10.1016/j.yebeh.2020.107687.

Xu, P., Huang, R., Wang, J., Van Dam, N.T., Xie, T., Dong, Z., Chen, C., Gu, R., Zang, Y.F., He, Y., Fan, J., Luo, Y.jia, 2014. Different topological organization of human brain functional networks with eyes open versus eyes closed. Neuroimage 90, 246–255. doi:10.1016/j.neuroimage.2013.12.060.

Yacoub, E., Grier, M.D., Auerbach, E.J., Lagore, R.L., Harel, N., Adriany, G., Zilverstand, A., Hayden, B.Y., Heilbronner, S.R., Uğurbil, K., Zimmermann, J., 2020. Ultra-high field (10.5 T) resting state fMRI in the macaque. Neuroimage 223. doi:10.1016/j.neuroimage.2020.117349.

Yacoub, E., Shmuel, A., Pfeuffer, J., Van De Moortele, P.F., Adriany, G., Andersen, P., Thomas Vaughan, J., Merkle, H., Ugurbil, K., Hu, X., 2001. Imaging brain function in humans at 7 Tesla. Magn. Reson. Med. 45, 588–594. doi:10.1002/mrm.1080.

Yacoub, E., Van De Moortele, P.F., Shmuel, A., Uğurbil, K., 2005. Signal and noise characteristics of Hahn SE and GE BOLD fMRI at 7 T in humans. Neuroimage 24, 738–750. doi:10.1016/j.neuroimage.2004.09.002.

Yancey, S.E., Rotenberg, D.J., Tam, F., Chiew, M., Ranieri, S., Biswas, L., Anderson, K.J., Baker, S.N., Wright, G.A., Graham, S.J., 2011. Spin-history artifact during functional MRI: potential for adaptive correction. Med. Phys. 38, 4634–4646. doi:10.1118/1.3583814.

Yang, J., Gohel, S., Vachha, B., 2020. Current methods and new directions in resting state fMRI. Clin. Imaging 65, 47–53. doi:10.1016/j.clinimag.2020.04.004.

Yang, Q.X., Mao, W., Wang, J., Smith, M.B., Lei, H., Zhang, X., Ugurbil, K., Chen, W., 2006. Manipulation of image intensity distribution at 7.0 T: passive RF shimming and focusing with dielectric materials. J. Magn. Reson. Imaging 24, 197–202. doi:10.1002/jmri.20603.

Yang, Q.X., Wang, J., Zhang, X., Collins, C.M., Smith, M.B., Liu, H., Zhu, X.H., Vaughan, J.T., Ugurbil, K., Chen, W., 2002. Analysis of wave behavior in lossy dielectric samples at high field. Magn. Reson. Med. 47, 982–989. doi:10.1002/mrm.10137.

Yeo, B.T.T., Krienen, F.M., Sepulcre, J., Sabuncu, M.R., Lashkari, D., Hollinshead, M., Roffman, J.L., Smoller, J.W., Zöllei, L., Polimeni, J.R., Fisch, B., Liu, H., Buckner, R.L., 2011. The organization of the human cerebral cortex estimated by intrinsic functional connectivity. J. Neurophysiol. 106, 1125–1165. doi:10.1152/jn.00338.2011.

Yun, S.D., Weidner, R., Weiss, P.H., Shah, N.J., 2019. Evaluating the utility of EPIK in a finger tapping fMRI experiment using BOLD detection and effective connectivity. Sci. Rep. 9, 1–11. doi:10.1038/s41598-019-47341-y.

Zahneisen, B., Hugger, T., Lee, K.J., LeVan, P., Reisert, M., Lee, H.L., Asslander, J., Zaitsev, M., Hennig, J., 2012. Single shot concentric shells trajectories for ultra fast fMRI. Magn. Reson. Med. 68, 484–494. doi:10.1002/mrm.23256.

Zaitsev, M., Akin, B., LeVan, P., Knowles, B.R., 2017. Prospective motion correction in functional MRI. Neuroimage 154, 33–42. doi:10.1016/j.neuroimage.2016.11.014.

Zaitsev, M., Zilles, K., Shah, N.J., 2001. Shared κ-space echo planar imaging with keyhole. Magn. Reson. Med. 45, 109–117 https://doi.org/10.1002/1522-2594(200101)45:1<109::AID-MRM1015>3.0.CO;2-X.

Zalesky, A., Fornito, A., Cocchi, L., Gollo, L.L., Breakspear, M., 2014. Time-resolved resting-state brain networks. Proc. Natl. Acad. Sci. USA 111, 10341–10346. doi:10.1073/pnas.1400181111.

Zhang, K., Huang, D., Shah, N.J., 2018. Comparison of resting-state brain activation detected by BOLD, blood volume and blood flow. Front. Hum. Neurosci. 12, 1–10. doi:10.3389/fnhum.2018.00443.

Zhu, J., Zhuo, C., Qin, W., Xu, Y., Xu, L., Liu, X., Yu, C., 2015. Altered resting-state cerebral blood flow and its connectivity in schizophrenia. J. Psychiatr. Res. 63, 28–35. doi:10.1016/j.jpsychires.2015.03.002.

Zou, Q., Miao, X., Liu, D., Wang, D.J.J., Zhuo, Y., Gao, J.H., 2015. Reliability comparison of spontaneous brain activities between BOLD and CBF contrasts in eyes-open and eyes-closed resting states. Neuroimage 121, 91–105. doi:10.1016/j.neuroimage.2015.07.044.

Zuo, Z., Wang, R., Zhuo, Y., Xue, R., Lawrence, K.S.S., Wang, D.J.J.J., St. Lawrence, K.S., Wang, D.J.J.J., 2013. Turbo-FLASH based arterial spin labeled perfusion MRI at 7 T. PLoS One 8, 1–9. doi:10.1371/journal.pone.0066612.